

# Magnetic Suppression of Cosmic Rays' Flux in $f(R)$ and $f(Q)$ Theories of Gravity

Swaraj Pratim Sarmah<sup>\*</sup> and Umananda Dev Goswami<sup>†</sup>  
*Department of Physics, Dibrugarh University, Dibrugarh 786004, Assam, India*

We investigate the effects of magnetic diffusion on the spectrum of ultra-high energy cosmic rays (UHECRs) from a cosmological perspective. To this end, we consider two modified theories of gravity (MTGs), namely, the  $f(R)$  gravity and a symmetric teleparallel gravity, also known as  $f(Q)$  gravity. Utilizing these two MTGs, we calculate the suppression in the flux of UHECRs for a collection of sources. Non-evolution (NE) and cosmic star formation rate (SFR) scenarios have been considered in our calculation of the suppression factor. This study also includes a mixed composition scenario involving the nuclei upto iron (Fe). Furthermore, we provide a parameterization of the suppression factor for the proton and also for the mixed compositions within the  $f(R)$  and  $f(Q)$  theories, considering both NE and SFR scenarios. The influence of the turbulent magnetic field on the suppression factor is also incorporated in our work. Comparative analysis of all our results with the standard  $\Lambda$ CDM model reveals significant effects of MTGs on the suppression factor that the  $f(R)$  power-law model predicts the lowest suppression factor, while the  $f(Q)$  model predicts the highest, and interestingly the results from the standard model fall within the range predicted by these two cosmological models.

Keywords: Ultra-High Energy Cosmic Rays; Flux; Suppression; Modified Gravity Theory

## I. INTRODUCTION

In the annals of physics, the 1912 discovery of cosmic rays (CRs) by V. F. Hess stands as a pivotal chapter [1]. CRs are charged particles, consisting of protons, helium, and heavier ions up to iron. Despite more than a century-spanning quest since their unveiling, the origin and propagation mechanisms of CRs through the Universe largely remain shrouded in mystery [2–4], with their narrative becoming most obscure beyond the energetic threshold of  $E \geq 0.1$  EeV ( $1 \text{ EeV} = 10^{18} \text{ eV}$ ). The provenance of these enigmatic ultra-high energy CRs (UHECRs) eludes our grasp [5–8]. Yet, for those within the more modest energy confines of  $E < 0.1$  EeV, supernovae within the galactic bounds are believed to be the celestial forges of acceleration [9–13]. Ascend higher, to realms around 1 EeV and beyond, and one enters the extragalactic domain, are supposed to be accelerated by gamma-ray bursts or active galactic nuclei [2].

The CR energy spectrum is a vast continuum, stretching from the GeV scale to the lofty heights of 100 EeV, tracing a power-law spectrum. Along this spectrum, a subtle inflection known as the ‘knee’ emerges at roughly  $4 \times 10^{15}$  eV, and a ‘second knee’ where the spectrum steepens more at around  $10^{17}$  eV [14, 15], followed by a flattening at the ‘ankle’ near  $5 \times 10^{18}$  eV. And then, near  $5 \times 10^{19}$  eV, one obtains the Greisen-Zatsepin-Kuzmin (GZK) cutoff—a stark demarcation in the CR spectrum [16–19]. CRs are the silent voyagers of space, carrying energies that dwarf those produced by any human-made accelerator, a fact that has intrigued and challenged physicists [20]. These particles, arriving at a rate of about one per square kilometer per century with energies exceeding  $6 \times 10^{19}$  eV [20], are the messengers from the unknown, holding secrets to questions that have persisted for more than a century. The pursuit of understanding these cosmic wanderers has led to significant advancements in experimental physics, revealing a surprising decrease in the flux of CRs above  $4 \times 10^{19}$  eV [21], contrary to earlier predictions. This suppression, confirmed by multiple studies [20–23], suggests a transition from lighter to heavier particles as energies increase, hinting at profound processes occurring over cosmological distances. It can also be understood by the source intensity population in the context of Hillas plot [24–26]. This plot relates the maximum energy at which a source can accelerate particles to its size and magnetic field strength, highlighting that only certain astrophysical environments are capable of accelerating heavy nuclei to the observed energies [25]. Such observations, including the setting of the upper limits on the presence of photons [20, 27, 28], neutrinos [20, 29, 30], and neutrons [20, 31] among these UHECRs, have been crucial in our quest to understand the universe. The observations of a shift in composition at energies beyond  $3 \times 10^{18}$  eV [32, 33] and a suppression in the flux above  $4 \times 10^{19}$  eV, which could be indicative of the GZK cutoff—a theoretical prediction of energy loss over vast intergalactic travels, were made nearly sixty years ago [18, 19]. However, despite these insights, the complete story of CRs remains elusive, as current data is insufficient to confirm if energy loss during propagation is the sole cause of this suppression.

The vast intergalactic stage is set with turbulent magnetic fields (TMFs), playing a pivotal role in the propagation of UHECRs. These charged particles, propelled from distant galaxies, find their paths intricately influenced by the TMFs they encounter. The path of a UHECR through space is a delicate balance between its traversed distance and the scattering length  $l_D = 3D/c$ , where  $D$  represents the diffusion coefficient and  $c$  is the speed of light [34]. When the cosmic path is shorter than  $l_D$ , the

\* Email: [rs\\_swarajpratimsarmah@dibru.ac.in](mailto:rs_swarajpratimsarmah@dibru.ac.in)

† Email: [umananda@dibru.ac.in](mailto:umananda@dibru.ac.in)

particle's journey is ballistic. On the other hand, if the distance greatly exceeds  $l_D$ , the particle's movement becomes diffusive. The inclusion of extragalactic TMFs and the finite density of cosmic sources can lead to a magnetic horizon effect due to which the CR flux is suppressed for decreasing energies [35]. This effect may reconcile observations with a higher spectral index [11, 36, 37], aligning with the theoretical values derived from diffusive shock acceleration. Another intriguing possibility involves the acceleration of heavy nuclei by extragalactic sources. These nuclei, upon interacting with the ambient infrared radiation (IR), undergo photodisintegration. This process releases a cascade of secondary nucleons, potentially explaining the lighter composition observed below the cosmic ankle [38, 39]. Intergalactic magnetic fields exert a profound influence on CRs, not only altering their trajectories but also potentially shaping their energy distribution. This latter effect, known as the magnetic horizon effect, manifests when magnetic fields are sufficiently intense to bar lower-energy CRs from reaching Earth, thereby reshaping the energy spectrum [40–43]. The extent of this influence hinges on the magnetic field's strength and the average spacing between CR sources. The propagation theorem [44] posits that magnetic fields do not impact the particle spectrum if source distances are significantly less than both the diffusion and attenuation lengths. Yet, in scenarios where magnetic fields are substantial and CR sources are sparsely scattered, a notable suppression in the low-energy end of the spectrum is anticipated. This suppression has previously been studied in Ref. [36] at the low energy case. In Ref. [45], the authors have studied the suppression by both analytic and numerical approaches for the primary and secondary nuclei.

Albert Einstein's General Relativity (GR), formulated in 1915, stands as a pinnacle of theoretical physics, elegantly describing gravitational phenomena. A century later, the LIGO collaboration confirmed Einstein's prediction of Gravitational Waves (GWs) [46], and the Event Horizon Telescope captured the first image of a black hole [47–52], both are monumental affirmations of GR. However, GR's inability to reconcile with quantum mechanics and account for the universe's accelerated expansion [53–57] with dark energy [58–62] and dark matter in galactic rotations [63–67] has led to the exploration of Modified Theories of Gravity (MTGs) [68, 69]. Among these, the  $f(R)$  gravity theory [70], which replaces the Ricci scalar  $R$  in the Einstein-Hilbert action by a function  $f(R)$ , has gained traction. Models like the Starobinsky [71, 72], Hu-Sawicki [73], Tsujikawa [74], and power-law [75, 76] models of  $f(R)$  gravity have been proposed to address these cosmic conundrums. Similarly, the symmetric teleparallel gravity and its extension, the  $f(Q)$  gravity are modifications of the standard teleparallel gravity theory, where the non-metricity scalar  $Q$  and its arbitrary function respectively replace the torsion scalar [77–81]. The  $f(Q)$  gravity has been used to investigate the cosmological implications, including the behaviour of dark energy, and has shown the potential to address cosmological tensions. Given MTGs' significant role in recent cosmological [82, 83] and astrophysical research [84–89], their application to UHECR studies, particularly in understanding the UHECR flux suppression, is a promising frontier. Till now, various research groups have studied the anisotropy [90–100], propagation mechanism [44, 101–107], and suppression [36, 45, 108, 109] of UHECRs from the standard cosmology as well as the observatories [110–121]. In our previous studies, we investigate the effects of  $f(R)$  gravity on the UHECRs' propagation [122] and anisotropy [123] for a single source system. In this work, we extend our previous studies of UHECRs for the diffusive suppression of UHECR flux for an ensemble of sources and some scenarios of mixed composition of nuclei including primary, secondary, and their intermediate nuclei, focusing on the  $f(R)$  and  $f(Q)$  gravity models for the very first time and compares their implications on UHECRs' suppression with the result from standard  $\Lambda$ CDM model.

The structure of this paper is organized as follows: In Section II, we delve into the intricate process of CR diffusion in the context of a turbulent magnetic field. Section III is neatly divided into two distinct parts. The first part introduces the  $f(R)$  power-law model, while the other part presents a  $f(Q)$  gravity model. In Section IV, we explore the suppression factor of the CR flux, leaving room for calculations involving multiple sources and a diverse composition of nuclei. The numerical results, along with their corresponding analytical fittings, are discussed in Section V. This is further divided into Subsection VA and Subsection VB, which deal with  $f(R)$  and  $f(Q)$  respectively. Finally, we wrap up our paper with a conclusive remark and a productive discussion in Section VI.

## II. DIFFUSIVE COSMIC RAYS IN TURBULENT MAGNETIC FIELDS

Creating a model for extragalactic magnetic fields is difficult due to limited observations [124]. The strength of these fields is not precisely known, which also varies across different regions [125, 126]. Near the cluster centers, field strengths range from several to tens of  $\mu\text{G}$  [124]. In less dense areas, they are weaker, typically between 1 and 10 nG, suggesting that significant fields may exist along the cosmic structures like filaments. Magnetic fields correlate with matter density, being stronger in dense regions such as superclusters and weaker in voids, possibly less than  $10^{-15}$  G. Moreover, the magnetic fields correlate with each other up to a maximum distance, known as the coherence length  $l_c$ . Estimates suggest that in our Local Supercluster, magnetic fields have coherence lengths from 10 kpc to 1 Mpc and RMS strengths between 1 and 100 nG [103]. The galactic magnetic field (GMF), with strengths of a few  $\mu\text{G}$ , influences CRs' travel paths but has a limited effect on their overall spectrum due to its smaller scale. In our Local Supercluster, the presence of strong magnetic fields are indicated by the observed polarised rotations of background sources, with estimated strengths of 0.3 to 2  $\mu\text{G}$  [3]. These fields are significant for CRs arriving from nearby sources. We simplify our study by focusing on CRs' movement through a uniform, turbulent extragalactic magnetic field. This field is characterized by its RMS strength  $B$  and coherence length  $l_c$ , with  $B$  defined as  $\sqrt{\langle B^2(x) \rangle}$  and ranging from 1 nG to

100 nG [127–129], while  $l_c$  spans from 0.01 Mpc to 1 Mpc [130]. The magnetic field within the Local Supercluster is crucial for understanding CRs' arrival on Earth, as it is most influential for CRs from nearby sources. Therefore, we exclude the effects of larger structures like filaments and voids.

A critical energy  $E_c$  can be defined as the energy where a charged particle's Larmor radius is equal to  $l_c$ , where the Larmor radius is given by

$$r_L = E/Z|e|B \simeq 1.1 \frac{E/\text{EeV}}{ZB/\text{nG}} \text{ Mpc},$$

and hence the critical energy  $E_c$  is given by  $E_c = Z|e|B l_c = 0.9Z (B/\text{nG}) (l_c/\text{Mpc}) \text{ EeV}$ . According to the MHD considerations  $B(z) = (1+z)B(0)$  and the  $l_c$  is assumed to be stretched by the expansion, so that  $l_c(z) = l_c(0)/(1+z)$  [3]. Here,  $B(0)$  and  $l_c(0)$  are the present values of  $B$  and  $l_c$  respectively.  $E_c$  distinguishes between two diffusion regimes: below  $E_c$ , resonant diffusion occurs, and above it, particles experience small deflections over  $l_c$ , leading to diffusion over much longer distances. When  $E < E_c$ , the Larmor radius  $r_L$  is smaller than the coherence length  $l_c$ , leading to diffusion through resonant scattering at wavelengths comparable to  $r_L$ . This is known as the quasi-linear regime. The diffusion length  $l_D$  is influenced by the magnetic field's strength at the Larmor radius scale, which is dependent on the turbulent magnetic field spectrum. Generally,  $l_D \approx l_c (E/E_c)^\alpha$ , where  $\alpha$  varies with the spectrum: 1/3 for Kolmogorov, 1/2 for Kraichnan, and 1 for Bohm diffusion, implying  $l_D = r_L$ .  $l_D$  is the distance over which a particle typically deflects by 1 radian, related to the random walk's basic step. The diffusion coefficient  $D(E)$  is  $c l_D/3$ , and the mean square displacement  $\langle (\Delta r)^2 \rangle$  after time  $\Delta t$  is  $6D\Delta t$  [36].

For  $E > E_c$  ( $r_L > l_c$ ), scattering is non-resonant, caused by several small deflections with each  $\sqrt{\delta\theta} \approx l_c/r_L$ . After  $N \approx l_D/l_c$  steps, the total deflection  $\Delta\theta \approx N\delta\theta = 1$  radian, yielding  $l_D \approx l_c (E/E_c)^2$ , indicating a rapid increase of diffusion length with energy. If  $l_D \ll r_s$  (the source distance), then spatial diffusion occurs; if  $l_D > r_s$ , the particles propagate quasi-rectilinearly, causing minor angular diffusion. A perfect fit to the diffusion coefficient was given by Ref. [2] as

$$D(E) \simeq \frac{c l_c}{3} \left[ 4 \left( \frac{E}{E_c} \right)^2 + a_I \left( \frac{E}{E_c} \right) + a_L \left( \frac{E}{E_c} \right)^\alpha \right], \quad (1)$$

and hence the diffusion length is given by

$$l_D(E) \simeq l_c \left[ 4 \left( \frac{E}{E_c} \right)^2 + a_I \left( \frac{E}{E_c} \right) + a_L \left( \frac{E}{E_c} \right)^\alpha \right], \quad (2)$$

where  $a_I$  and  $a_L$  are two constants.  $a_I \approx 0.9$  and  $a_L \approx 0.23$  according to the Kolmogorov spectrum, whereas as per the Kraichnan spectrum,  $a_I \approx 0.65$  and  $a_L \approx 0.42$  [2].

The average separation between the sources of UHECRs, denoted as  $d_s$ , is intrinsically linked to their density  $n_s$  and can be expressed as  $d_s \approx n_s^{-1/3}$  [36]. For a value of  $n_s = 10^{-3} \text{ Mpc}^{-3}$ , the separation is approximately  $d_s \approx 10 \text{ Mpc}$ . Consequently, for a lower density of  $n_s = 10^{-6} \text{ Mpc}^{-3}$ , the separation increases to  $d_s \approx 100 \text{ Mpc}$ .

The shaping of CR spectra for different elements is fundamentally influenced by two main factors: their interactions with radiation backgrounds and the impact of cosmological evolution. Energy losses in CRs are due to adiabatic losses, represented as  $dE/dt = -HE$ , where  $H = \dot{a}/a$  is the Hubble's parameter in terms of the scale factor  $a$ . These losses are prevalent across all energy levels and also result from interaction losses from various processes. Pair creation losses ( $e^+e^-$ ) become significant when interacting with Cosmic Microwave Background (CMB) photons of energy  $\epsilon \sim 10^{-3} \text{ eV}$ . This requires CR Lorentz factor  $\Gamma > 10^9$ , which implies that  $E > A \text{ EeV}$  for nuclei with mass number  $A$ . For protons, the energy loss length becomes less than the Hubble horizon  $R_H = c/H_0$ , when proton energies exceed  $E_p > 2 \text{ EeV}$ . For heavier nuclei, due to an increased threshold and a larger pair production cross section ( $\sigma \propto Z^2$ ), the energy loss length becomes comparable to  $R_H$  when  $E_A \approx A \text{ EeV}$  [131]. The process of photo-pion production becomes noticeable only at extremely high energies, specifically when  $E/A > 50 \text{ EeV}$ . Photo-disintegration of nuclei comes into play for  $E > 2A \text{ EeV}$  when interacting with CMB photons, and even at lower energies when interacting with higher energy background photons, such as those in the IR range. However, when interacting with IR photons, the energy loss length for photo-disintegration exceeds the Hubble horizon, except for heavier nuclei like Iron (Fe). For these heavier nuclei, the energy loss length is larger than  $R_H$  only when  $E < 30 \text{ EeV}$  [131]. Generally, for energies less than  $E < Z \text{ EeV}$ , the main energy losses are due to adiabatic effects, while interaction losses are minor [36]. Besides adiabatic losses, cosmological influences also contribute to the increase in CMB density and temperature with redshift. These influences may also affect the evolution of other radiation backgrounds, the density and emissivity of CR sources, and possibly the evolution of magnetic fields. Some additional mechanisms like the GZK effect, photodissociation, and pair production become increasingly important, especially for specific particle compositions and interactions with cosmic background radiation. The cosmological models also have some effects on the propagation of UHECRs. In the next section, we will discuss the cosmological models used for this work.

### III. COSMOLOGICAL MODELS

In this section, we will discuss the cosmological models that will be used in the calculations for the different parameters needed for this current work. For this purpose, we consider one model from each of the two modified gravity theories:  $f(R)$  and  $f(Q)$ . We will also introduce the Hubble parameter  $H(z)$  in this section for the models of both modified gravity theories.

#### A. $f(R)$ gravity model

We consider here the simplest model, the  $f(R)$  gravity power-law model, whose functional form is [75, 76, 132]

$$f(R) = \beta R^n, \quad (3)$$

where  $\beta$  and  $n$  are model parameters. The parameter  $\beta$  has the dependence on the value of  $n$  and other cosmological parameters such as Hubble constant  $H_0$ , current matter density parameter  $\Omega_{m0}$  and also radiation density parameter  $\Omega_{r0}$  via Ricci scalar at present time  $R_0$  as given by [132]

$$\beta = -\frac{3H_0^2 \Omega_{m0}}{(n-2)R_0^n}, \quad (4)$$

where the expression for  $R_0$  is given by [132]

$$R_0 = -\frac{3(3-n)^2 H_0^2 \Omega_{m0}}{2n[(n-3)\Omega_{m0} + 2(n-2)\Omega_{r0}]}. \quad (5)$$

By using the Palatini formalism, the Friedmann equation in  $f(R)$  theory in terms of redshift  $z$  can be written as [133]

$$\frac{H^2}{H_0^2} = \frac{3\Omega_{m0}(1+z)^3 + 6\Omega_{r0}(1+z)^4 + \frac{f(R)}{H_0^2}}{6f'(R)\zeta^2}, \quad (6)$$

where

$$\zeta = 1 + \frac{9f''(R)}{2f'(R)} \frac{H_0^2 \Omega_{m0}(1+z)^3}{Rf'(R) - f''(R)}. \quad (7)$$

Thus, from Eqs. (6) and (7), we can express the Hubble parameter as a function of the redshift  $z$  as

$$H(z) = \left[ -\frac{2nR_0}{3(3-n)^2 \Omega_{m0}} \left\{ (n-3)\Omega_{m0}(1+z)^{\frac{3}{n}} + 2(n-2)\Omega_{r0}(1+z)^{\frac{n+3}{n}} \right\} \right]^{\frac{1}{2}}. \quad (8)$$

In our current study, we take the value of the model parameter  $n = 1.4$ , which is the best-fitted value for the model as analyzed in Ref. [132]. The values of the other cosmological parameters used in this study are taken as  $H_0 \approx 67.4 \text{ km s}^{-1} \text{ Mpc}^{-1}$  [134],  $\Omega_{m0} \approx 0.315$  [134], and  $\Omega_{r0} \approx 5.373 \times 10^{-5}$  [135]. Thus the relation between cosmological time evolution and redshift can be expressed as [122]

$$\left. \frac{dt}{dz} \right|_{f(R)} = \frac{1}{(1+z)H} = (1+z)^{-1} \left[ -\frac{2nR_0}{3(3-n)^2 \Omega_{m0}} \left\{ (n-3)\Omega_{m0}(1+z)^{\frac{3}{n}} + 2(n-2)\Omega_{r0}(1+z)^{\frac{n+3}{n}} \right\} \right]^{-\frac{1}{2}}. \quad (9)$$

This relation will be used to calculate the CR flux for this model of  $f(R)$  gravity in Section IV.

#### B. $f(Q)$ gravity model

We consider the functional form of the  $f(Q)$  gravity in this work as [136]

$$f(Q) = \sigma Q, \quad (10)$$

where  $\sigma$  is the model parameter. For this  $f(Q)$  gravity model, the Hubble parameter in terms of the redshift  $z$  can be written as [136]

$$H(z) = H_0 \left[ (1+z)^{\frac{3\sigma+C_1+C_2}{2\sigma+C_2}} \left( 1 + \frac{C_0}{3\sigma+C_1+C_2} \right) - \frac{C_0}{3\sigma+C_1+C_2} \right], \quad (11)$$

where  $C_0$ ,  $C_1$  and  $C_2$  are three constant parameters, considered as bulk viscous parameters. The best-fitted values of all these model parameters are  $\sigma = -1.03_{-0.55}^{+0.52}$ ,  $C_0 = 1.54_{-0.79}^{+0.83}$ ,  $C_1 = 0.08_{-0.49}^{+0.49}$ , and  $C_2 = 0.66_{-0.83}^{+0.82}$  as reported in the Ref. [136]. As in the previous case, the relation between cosmological time evolution and redshift can be expressed for this  $f(Q)$  gravity model as

$$\left. \frac{dt}{dz} \right|_{f(Q)} = (H_0(1+z))^{-1} \left[ (1+z)^{\frac{3\sigma+C_1+C_2}{2\sigma+C_2}} \left( 1 + \frac{C_0}{3\sigma+C_1+C_2} \right) - \frac{C_0}{3\sigma+C_1+C_2} \right]^{-1}. \quad (12)$$

In Section IV we will use this relation to calculate the CR flux for this model of  $f(Q)$  gravity.

In the left panel of Fig. 1, we plot the Hubble parameters for the  $f(R)$  gravity power-law model and the  $f(Q)$  gravity model using Eqs. (8) and (11) respectively considering the respective set of model parameters as mentioned above along with the Hubble parameter for the standard  $\Lambda$ CDM model. We compare the results with the observational Hubble data (OHD) obtained from differential age (DA) and Baryon Acoustic oscillations (BAO) methods [122, 132, 136]. As one can see from this plot, both modified gravity models are well-fitted with the observational data. However, it needs to be mentioned that all three models predict slightly different values of Hubble constant  $H_0$  as  $67.77 \text{ km s}^{-1} \text{ Mpc}^{-1}$  ( $\Lambda$ CDM),  $68.4 \text{ km s}^{-1} \text{ Mpc}^{-1}$  ( $f(R)$  power-law) and  $69.0 \text{ km s}^{-1} \text{ Mpc}^{-1}$  ( $f(Q)$  model) respectively [136]. It is clear that values for the  $\Lambda$ CDM and  $f(R)$  power-law model are very close to the observed value of  $H_0$  by the Planck experiment [134]. For completeness, we also plot the cosmological time evolution with respect to redshift  $z$  for all three models of gravity considered as above in the right panel of Fig. 1. From this plot, one can see that at the present value of redshift i.e. at  $z = 0$ , there are no significant differences in the predictions of considered cosmological models. However, as the value of  $z$  increases, the differences become more pronounced, especially with the  $f(R)$  gravity power-law model. Whereas at  $z = 2.5$ , the  $\Lambda$ CDM and  $f(R)$  power-law models tend to converge, while the  $f(Q)$  model follows a flat pattern.

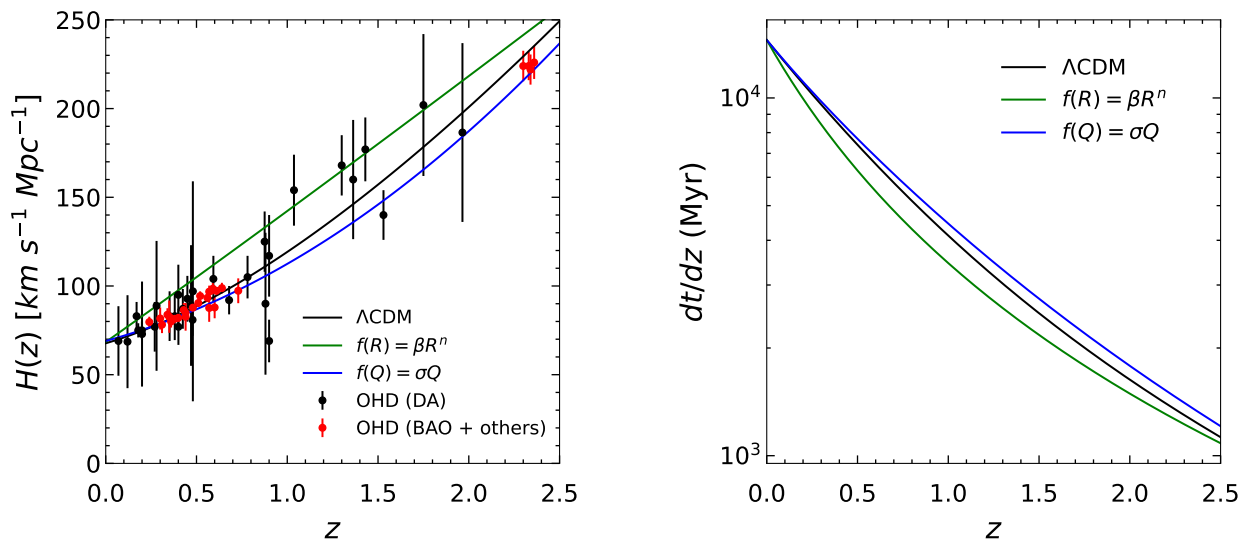


FIG. 1. Left: Variations of Hubble parameter  $H(z)$  with redshift  $z$  as predicted by the  $\Lambda$ CDM model,  $f(R)$  gravity power-law model, and the  $f(Q)$  gravity model in comparison with the observational Hubble data (OHD) obtained from differential age (DA) and Baryon Acoustic oscillations (BAO) methods [122, 132, 136]. Right: Evolution of cosmological time with  $z$  as predicted by the aforementioned models of gravity.

In the following section, we will apply these cosmological models to understand CR flux suppression. In this context, another pertinent point to be mentioned here is that variation of  $H_0$  values for different models will not affect the CR flux suppression as it is independent of  $H_0$ . This will be clear in the following section.

#### IV. THE SUPPRESSION OF CR FLUX

In the past, the diffusion of CRs in the TMF was discussed by several researchers [39, 104, 130, 137–145]. In the expanding Universe, a detailed analysis has been performed generalising the Syrovatskii solution [146] for a proton diffusion by Berezhinsky and Gazizov [41, 104]. The proton flux anticipated from a CR source at a distance of  $r_s$ , significantly exceeding the diffusion length  $l_D$ , can be determined by solving the diffusion equation within the expanding Universe [104]. The resulting expression

is as follows [45]:

$$J(E) = \frac{c}{4\pi} \int_0^{z_{\max}} dz \left| \frac{dt}{dz} \right| \mathcal{L} [E_g(E, z), z] \frac{\exp[-r_s^2/4\lambda^2]}{(4\pi\lambda^2)^{3/2}} \frac{dE_g}{dE}, \quad (13)$$

where  $z_{\max}$  is the maximum redshift of the source at which it starts to emit CRs,  $E_g(E, z)$  is the generation energy at redshift  $z$  whose value is  $E$  at  $z = 0$ ,  $\mathcal{L}$  is the source emissivity that is obtained by summing up the contributions of the charge specific emissivity  $\mathcal{L}_Z$  from various charges. We will employ a power-law with a rigidity cutoff  $ZE_{\max}$ , represented as  $\mathcal{L}_Z(E, z) = \xi_Z f(z) E^{-\gamma} / \cosh(E/ZE_{\max})$  [36]. Here  $\xi_Z$  represents the relative contribution to the CRs flux of charge  $Z$  nuclei and  $f(z)$  denotes the source emissivity evolution concerning the redshift  $z$ . Since  $H(z)$  varies across different cosmological models, the predictions made by these models will depend on the factor  $dt/dz$ , as described in Eqs. (9) and (12). The Styrovatskii variable  $\lambda^2$  is given by

$$\lambda^2(E, z) = \int_0^z dz \left| \frac{dt}{dz} \right| (1+z)^2 D(E_g, z). \quad (14)$$

Even though Eq. (13) was originally derived for protons, it can also be applied to nuclei by expressing it in terms of particle rigidities. When it comes to photo-disintegration processes in nuclei, they tend to conserve the Lorentz factor and rigidity of the main fragment. As a result, these processes do not significantly impact the particle's diffusion properties. However, there is a potential complication in relation to the photo-disintegration losses. As the source term  $\mathcal{L}$  should refer to the primary nucleus that led to the observed one, obtaining this information is challenging due to the stochastic nature of the process. In the past, S. Mollerach et al. discussed this scenario [36] and we will extend this work in a modified gravity framework. Since in this work, we are interested in multiple sources instead of a single source, so according to the propagation theorem [44], to sum all the sources, one can use

$$\int_0^\infty dr 4\pi r^2 \frac{\exp[-r^2/4\lambda^2]}{(4\pi\lambda^2)^{3/2}} = 1. \quad (15)$$

To understand how the finite distance to the sources affects suppression, we compute the sum using a specific set of distance distributions. These distributions correspond to a uniform source density, and we consider the source distances from the observer as  $r_i = (3/4\pi)^{1/3} d_s \Gamma(i+1/3)/(i-1)!$  [36, 45], where  $d_s$  is the distance between the sources and  $i$  corresponds to the  $i^{\text{th}}$  sources from an average distance. Hence, for a discrete source distribution, performing the sum over the sources, one can get a factor [36, 45]

$$F \equiv \frac{1}{n_s} \sum_i \frac{\exp[-r_i^2/4\lambda^2]}{(4\pi\lambda^2)^{3/2}} \quad (16)$$

instead of getting Eq. (15).

In Eq. (13), after summing all the sources, we can write the combined flux for an ensemble of sources for the  $f(R)$  gravity power-law model as

$$J_{\text{com}}(E) \Big|_{f(R)} \simeq \frac{R_H n_s}{4\pi} \int_0^{z_{\max}} dz (1+z)^{-1} \left[ -\frac{2nR_0}{3(3-n)^2 \Omega_{m0}} \left\{ (n-3)\Omega_{m0}(1+z)^{\frac{3}{n}} + 2(n-2)\Omega_{r0}(1+z)^{\frac{n+3}{n}} \right\} \right]^{-\frac{1}{2}} \\ \times \mathcal{L} [E_g(E, z), z] \frac{dE_g}{dE} F, \quad (17)$$

where  $R_H = c/H_0$  is the Hubble radius. Similarly, for the  $f(Q)$  gravity model, the combined flux can be written as

$$J_{\text{com}}(E) \Big|_{f(Q)} \simeq \frac{R_H n_s}{4\pi} \int_0^{z_{\max}} dz (1+z)^{-1} \left[ (1+z)^{\frac{3\sigma+C_1+C_2}{2\sigma+C_2}} \left( 1 + \frac{C_0}{3\sigma+C_1+C_2} \right) - \frac{C_0}{3\sigma+C_1+C_2} \right]^{-1} \\ \times \mathcal{L} [E_g(E, z), z] \frac{dE_g}{dE} F. \quad (18)$$

The final suppression factor of CR flux that describes the magnetic horizon effect can be expressed as

$$G(E/E_c) \equiv \frac{J_{\text{com}}(E)}{J_{\text{com}}(E) \Big|_{d_s \rightarrow 0}}, \quad (19)$$

which is the ratio of the actual flux from discrete source distribution to that of the continuous source distribution ( $d_s \rightarrow 0$ ). The continuous source distribution corresponds to the term  $F = 1$  in Eqs. (17) and (18), and it means that the flux is independent of the modes of propagation of CRs. Moreover, we can rewrite the Eq. (14) in terms of Hubble radius  $R_H$  and from Eq. (1) as

$$\lambda^2(E, z) = H_0 \frac{R_H l_c}{3} \int_0^z dz \left| \frac{dt}{dz} \right| (1+z)^2 \left[ 4 \left( \frac{(1+z)E}{E_c} \right)^2 + a_I \left( \frac{(1+z)E}{E_c} \right) + a_L \left( \frac{(1+z)E}{E_c} \right)^\alpha \right]. \quad (20)$$

The suppression factor relies on the coherence length  $l_c$  and the distance between the sources  $d_s$  by this following relation [36, 147]

$$X_s = \frac{d_s}{\sqrt{R_H l_c}}. \quad (21)$$

This relation  $X_s$  is known as the finite density factor and it will appear in the factor  $F$  given in Eq. (16) after using Eq. (20) in it. Hence  $X_s$  will be used in Eq. (17) and Eq. (18) while running the numerical calculations. In the next section, we will discuss the results obtained from the computations of Eq. (19) for different scenarios.

## V. NUMERICAL ANALYSIS

This section is completely devoted to the numerical simulation and their corresponding analytic fitting. It is divided into two subsections for a systematic analysis: the first subsection for the  $f(R)$  gravity model and the latter one for the model of  $f(Q)$  gravity. We extensively use the `python scipy` library [148] for the calculation with some assistance from the `CRPropa 3.2` [149] and `SimProp v2r4` [150] codes. Unless we specify, we use the RMS value of the magnetic field as 1 nG, the coherence length of 1 Mpc, and the spectral index  $\gamma = 2$  in all of the following plots.

### A. Results from $f(R)$ gravity model

In the left panel of Fig. 2, we plot the suppression factor  $G$  vs  $E/E_c$  that is obtained by the magnetic horizon effect considering the maximum redshift of  $z_{\max} = 2$ . Here, we consider the finite density factor  $X_s = 0.5, 1, 2$  and 3. As this factor is increasing, the departure of the suppression factor is clearly seen. The filled dots represent the numerical simulation of the  $f(R)$  model, while the hollow dots are for the  $\Lambda$ CDM model. The difference between the  $f(R)$  model and the standard  $\Lambda$ CDM model is visible in this plot. The flux is less comparatively suppressed in the  $f(R)$  gravity model. The solid lines represent the corresponding fits for the  $f(R)$  gravity model, while the dotted lines for the  $\Lambda$ CDM model. We adopt the method of Ref. [45] for the fitting formalism, but our parameterizations are a little bit different. The fitting equation that is used in the whole work is given by [45]

$$P(x) = \exp \left[ - \left( \frac{a X_s}{x + b(x/a)^\eta} \right)^\vartheta \right], \quad (22)$$

where  $a$ ,  $b$ ,  $\vartheta$  and  $\eta$  are fitting parameters. The parameterizations required for fitting the expression throughout this work are given in Table I. In the right panel of Fig. 2, we plot the same results as the left panel, but with a zoomed view in a small-scale region. It is seen that although the suppressions seem the same between the  $E/E_c$  ranges of 1 to 100 in the left panel, in the zoomed view of the same on the right panel, they are not exactly the same.

The suppression factor generally depends on the luminosity evolution of the sources with respect to the redshift. In Fig. 2, we have adopted the constant luminosity source evolution i.e. no cosmological evolution (NE). For the cosmological evolution star formation rate (SFR) we adopt the formalism as follows [151]:

$$\mathcal{L} \propto \begin{cases} (1+z)^{3.44}, & \text{if } z \leq 0.97 \\ (1+z)^{-0.26}, & \text{if } 0.97 < z \leq 4.48 \\ (1+z)^{-7.8}, & \text{if } z > 4.48 \end{cases} \quad (23)$$

For this SFR case, we simulate the suppression factor upto  $z_{\max} = 4$ . In Fig. 3, we plot the SFR scenario (filled and hollow triangle) along with the non-evolution (filled and hollow circle) case. Here, the hollow points represent the results from the  $\Lambda$ CDM model and those of filled ones represent the  $f(R)$  gravity power-law model. For a certain energy, the cosmic particles arrive from a higher redshift in the SFR case than that of the NE case [45]. Here also the  $f(R)$  gravity model is less suppressed in the lower energy region as well as in the higher energy range. The middle region suppression is similar (although not exactly the same as we have already shown in the right panel of Fig. 2) for the both  $f(R)$  model and the standard  $\Lambda$ CDM model. The

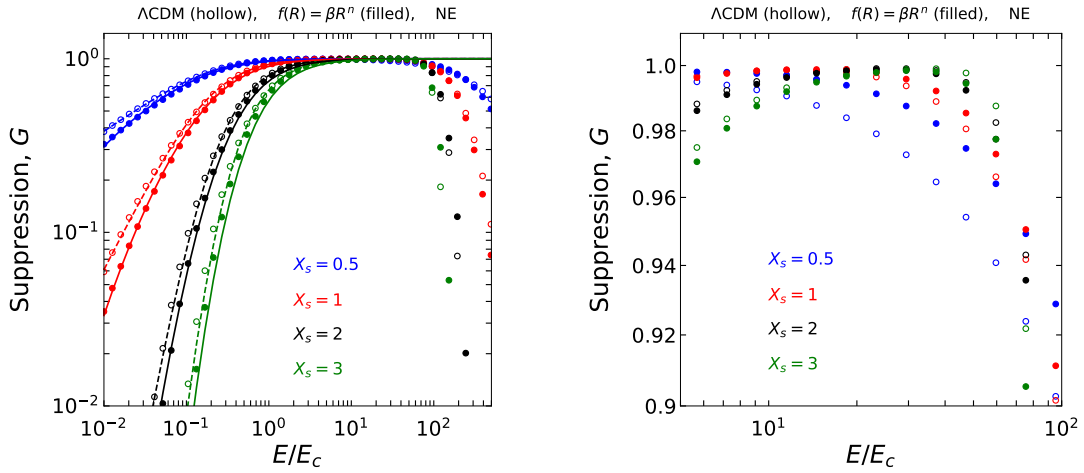


FIG. 2. Left: Suppression factors for different finite density factors of sources  $X_s$  as predicted by the  $\Lambda$ CDM model and the  $f(R)$  gravity power-law model. The dotted and solid lines are for the analytic fitting for these two cosmological models respectively. Right: Same as the left panel but for a small scaling region. Both these plots are for the no cosmological evolution (NE) scenario. In the plots the hollow symbol represents the  $\Lambda$ CDM model and the filled symbol represents the  $f(R)$  gravity power-law model. This representation will be followed in the rest of similar figures.

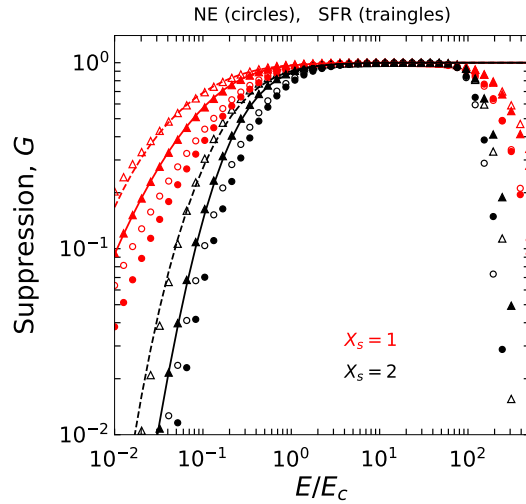


FIG. 3. Suppression factors for two different finite density factors of sources  $X_s = 1$  (red points) and  $X_s = 2$  (black points) as predicted by the  $\Lambda$ CDM model and the  $f(R)$  gravity power-law model. The hollow and filled points represent the results from the  $\Lambda$ CDM model and the  $f(R)$  gravity power-law model respectively. The circle and triangle in the plot represent the NE and SFR scenarios respectively. The solid and dotted lines represent the analytic fitting for the said cosmological models.

TABLE I. Parametrizations of Eq. (22) for the  $\Lambda$ CDM model and the  $f(R)$  gravity power-law model with NE and SFR scenarios.

NE							
$\Lambda$ CDM				$f(R)$ model			
a	b	$\vartheta$	$\eta$	a	b	$\vartheta$	$\eta$
0.224	0.162	1.541	0.140	0.305	0.262	1.55	0.210
SFR							
$\Lambda$ CDM				$f(R)$ model			
a	b	$\vartheta$	$\eta$	a	b	$\vartheta$	$\eta$
0.215	0.334	1.810	0.270	0.202	0.163	1.800	0.190



solid and the dashed lines represent the fitting of Eq. (22) for the  $f(R)$  and  $\Lambda$ CDM models respectively. The fitting parameters for the  $f(R)$  power-law model and  $\Lambda$ CDM model each with the NE and SFR cases are given in Table I.

As we can see from Figs. 2 and 3 a change in suppression at higher energies is also evident and this suppression is mainly due to the radiation backgrounds. When the energy exceeds 60 EeV, the attenuation length of protons decreases rapidly due to the photopion production with the CMB, falling significantly below 100 Mpc for energies greater than 100 EeV [45]. A similar phenomenon occurs for heavier nuclei at energies exceeding approximately  $5Z$  EeV, as a result of the photodisintegrations with the CMB photons [45]. In simple words, when the energy reaches a point where the attenuation length is about the same or less than the distance to the nearest sources, we see a significant decrease in the flux. This scenario is seen clearly in Fig. 4. For this computation, we take the different primaries from  $Z = 1$  upto  $Z = 26$ . We consider  $Z = 7$  for the CNO group,  $Z = 14$  for the Si group, and  $Z = 26$  for the Fe group. The left panel of Fig. 4 is for the NE scenario, while the right panel is for the SFR by considering  $X_s = 1$ . It is to be noted that the cosmological model effect is more evident in SFR than in the NE case. Here also the same results are obtained as in the earlier case that the  $f(R)$  model exhibits a lower suppression in both high and low energy regimes than the  $\Lambda$ CDM model.

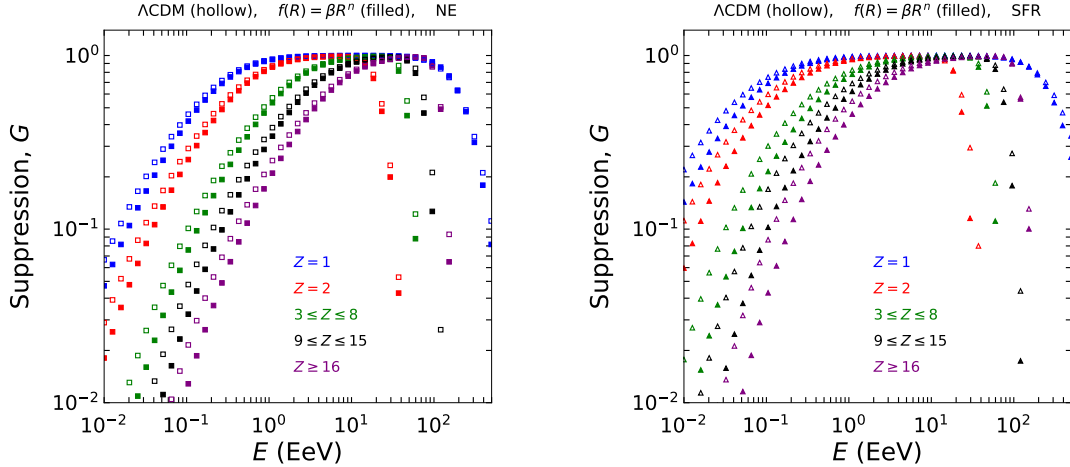


FIG. 4. Left: Variations of suppression factor with respect to the energy  $E$  for the different primaries as predicted by the  $\Lambda$ CDM model and the  $f(R)$  gravity model with NE and  $X_s = 1$ . Right: Same as the left pane but for the SFR case.

In Fig. 5, we also plot the suppression factor with respect to  $E/E_c$  for different nuclei. In the left panel, we plot the NE case, while the SFR case is plotted in the right panel. We can see that all nuclei show the same behaviour for their respective primaries. Again here the nuclei in the  $f(R)$  gravity model are less suppressed in comparison with the  $\Lambda$ CDM model. In the higher energy range, a sharp drop in flux appears which is mainly due to the photodisintegration.

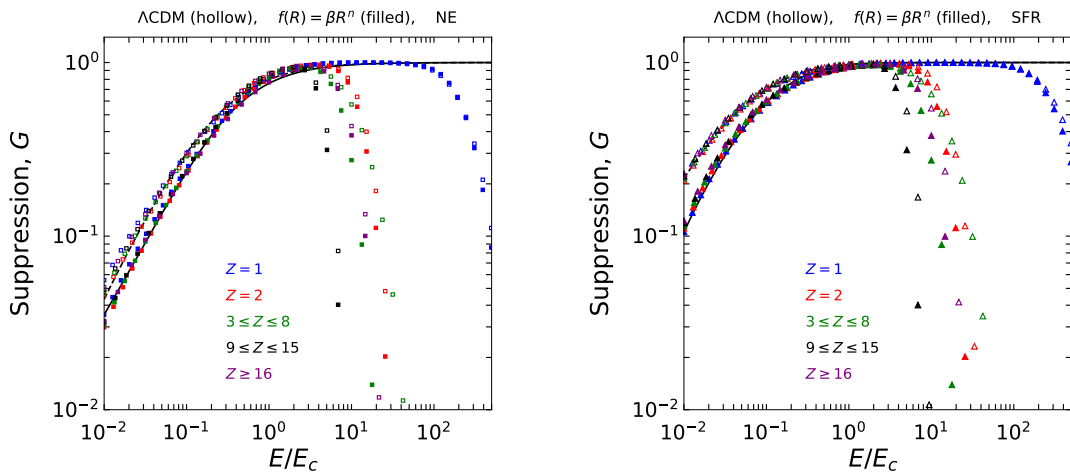


FIG. 5. Left: Variations of suppression factor with respect to  $E/E_c$  for the different primaries as predicted by the  $\Lambda$ CDM model and the  $f(R)$  gravity model with NE and  $X_s = 1$ . Right: Same as the left pane but for the SFR case.

In all the above scenarios, we consider the magnetic field strength  $B = 1$  nG. Now, the effect of a variation of the magnetic field strength in the suppression factor can be seen in Fig. 6. Here we consider the magnetic field strength from 1 nG to 15 nG.

In this figure, the left panel is for the NE case while the right one is for the SFR case. The cosmological model effect is the same as that of the earlier cases. At low energy levels, the predictions of the  $\Lambda$ CDM model at 15 nG closely align with those of the  $f(R)$  gravity power-law model at 10 nG. The variation of suppression factor between magnetic fields of strengths 1 nG to 5 nG is quite large as compared to that for the 5 nG to 15 nG. We also check (not included here) for the higher magnetic field strength such as 50 nG, but interestingly no significant variation can be seen as we see the variation for the 1 nG to 5 nG.

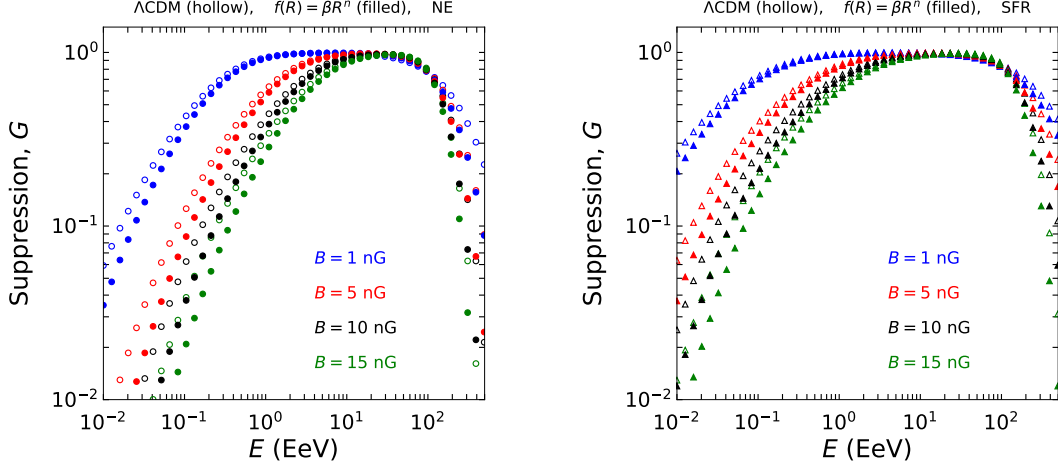


FIG. 6. Left: Variations of suppression factor with respect to energy  $E$  for different strengths of the magnetic field as predicted by the  $\Lambda$ CDM model and the  $f(R)$  gravity power-law model with NE and  $X_s = 1$ . Right: Same as the left pane but for the SFR case.

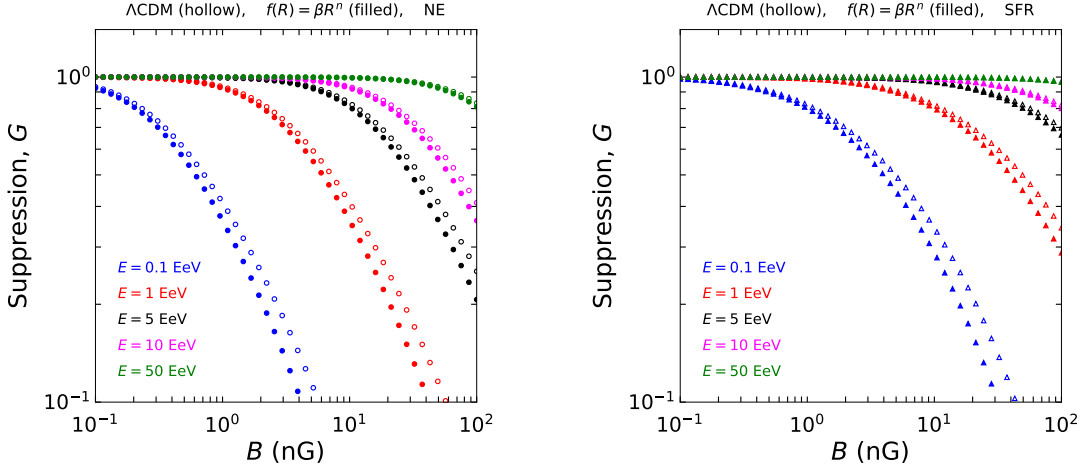


FIG. 7. Left: Variations of suppression factor with respect to the magnetic field for different energy values as predicted by the  $\Lambda$ CDM and the  $f(R)$  gravity power-law model with NE and  $X_s = 1$ . Right: Same as the left pane but for the SFR case.

For a more clear picture of the variation of the suppression factor with magnetic field strength, in Fig. 7, the flux suppression factor as a function of the magnetic field is plotted. For this scene, we take the energy values from  $E = 0.1$  EeV to  $E = 50$  EeV, and the NE and SFR cases are also shown in the left and right panels of this figure respectively. The standard  $\Lambda$ CDM model predicts higher suppression than the  $f(R)$  gravity power-law model as expected. The cosmological model's effect is evident throughout the plot, but as the TMF shifts to a higher strength, the model effect becomes more. It is seen that the suppression decreases quickly with increasing magnetic field for low energy particles and for substantially high energy particles it almost remains constant up to very high magnetic field strength. One important result to be noted is that the suppression predicted by the  $f(R)$  power-law model at  $E = 1$  EeV in the NE case is the same as the  $\Lambda$ CDM at  $E = 0.1$  EeV in the SFR case.

## B. Results from $f(Q)$ gravity model

Following the same procedures as discussed above, here we discuss the numerical results obtained from the  $f(Q)$  gravity model. Fig. 8 shows the variation of the suppression factor with respect to  $E/E_c$  as predicted by the  $f(Q)$  gravity model in

comparison with that of the  $\Lambda$ CDM model. In the left panel of the figure, we have shown the NE scenario while the SFR is shown in the right panel. In the plots, the empty circles or triangles are for the  $\Lambda$ CDM model while the filled ones are for the  $f(Q)$  gravity model.

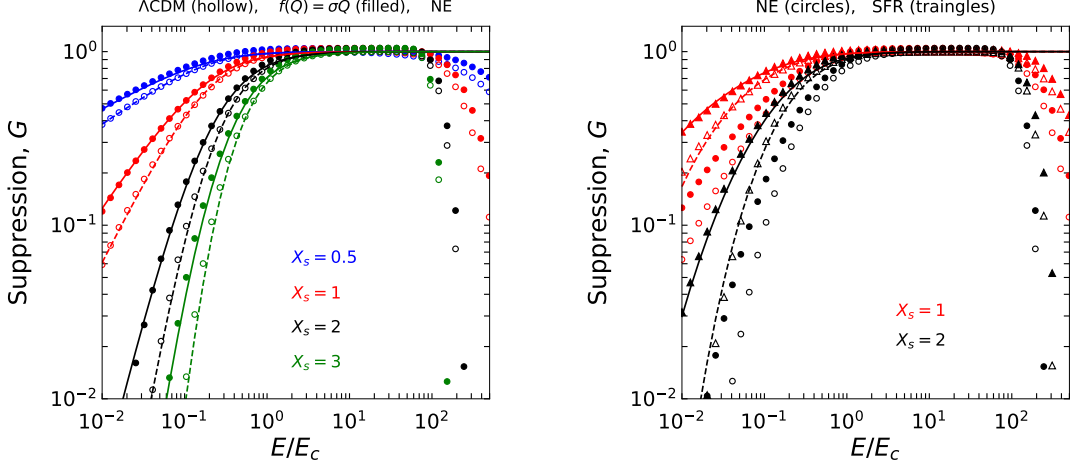


FIG. 8. Left: Suppression factors with respect to  $E/E_c$  for different density factors of sources  $X_s$  as predicted by the  $\Lambda$ CDM model and the  $f(R)$  gravity model. Right: The suppression factors for two different density factors of sources  $X_s = 1$  and  $X_s = 2$  as predicted by the  $\Lambda$ CDM model and the  $f(R)$  gravity model. The round and triangle-shaped points represent the NE and SFR scenarios respectively. The hollow and filled points represent the results from the  $\Lambda$ CDM model and the  $f(Q)$  gravity model respectively. The dotted and solid lines are for the analytic fitting for these two respective cosmological models.

TABLE II. Parametrizations of Eq. (22) for the  $f(Q)$  gravity model with NE and SFR scenario, and with  $\gamma = 2$ .

NE			
a	b	$\vartheta$	$\eta$
0.194	0.172	1.448	0.160
SFR			
a	b	$\vartheta$	$\eta$
0.175	0.301	1.710	0.231

Unlike the previous case of MTG, here the  $f(Q)$  gravity model depicts a higher suppression than that of the  $\Lambda$ CDM model. In the right panel, the red points are for the density factor of sources  $X_s = 1$  and the black points are for  $X_s = 2$ . The solid and dotted lines are for the corresponding fitting of the numerical results of the  $f(Q)$  gravity model and the  $\Lambda$ CDM model. We adopt the same Eq. (22) for the analytic fitting. The cosmological model's effect is more evident in the SFR case as compared to the NE case. The fitting parameters relevant to this calculation are given in Table II.

A mixed composition of nuclei upto iron is plotted in Fig. 9. The left panels of Fig. 9 are for the NE scenario, while the right panels are for the SFR by considering  $X_s = 1$ . Here also the same results are obtained as in the earlier case that the  $f(Q)$  model exhibits a higher suppression in both high and low energy regimes than the  $\Lambda$ CDM model. In the top panels of Fig. 9, we plot the suppression factor with respect to the energy for different nuclei. In the bottom panels of Fig. 9, we also plot the suppression factor with respect to  $E/E_c$  for the same nuclei. In the left panel, we plot the NE case, while the SFR case is plotted in the right panel. We can see that all nuclei show the same behaviour for their respective primaries when plotting with respect to  $E/E_c$ . Again here the nuclei in the  $\Lambda$ CDM model are less suppressed in comparison with the  $f(Q)$  model. A sharp drop in flux appears in higher energy cases due to the photodisintegration as we have already discussed in the previous section.

A discernible variation in the suppression factor with respect to the magnetic field strength is illustrated in Fig. 10. As in the previous case, the magnetic field strength under consideration ranges from 1 nG to 15 nG. In Fig. 10, the left panel corresponds to the NE case, while the right panel represents the SFR case. The influence of the cosmological model is consistent with previous cases. At lower energy levels, the  $\Lambda$ CDM model's predictions at 10 nG align closely with those of the  $f(Q)$  model at 15 nG. We will discuss these types of scenarios in the next section. The suppression factor exhibits a substantial variation between the magnetic field of strengths 1 nG and 5 nG, compared to the range from 5 nG to 15 nG. We also examined higher magnetic field strengths, such as 50 nG (results not included here). Interestingly, the variation observed in this range was not as significant as the variation from 1 nG to 5 nG. In Fig. 11, we present the flux suppression factor as a function of the strength of the magnetic

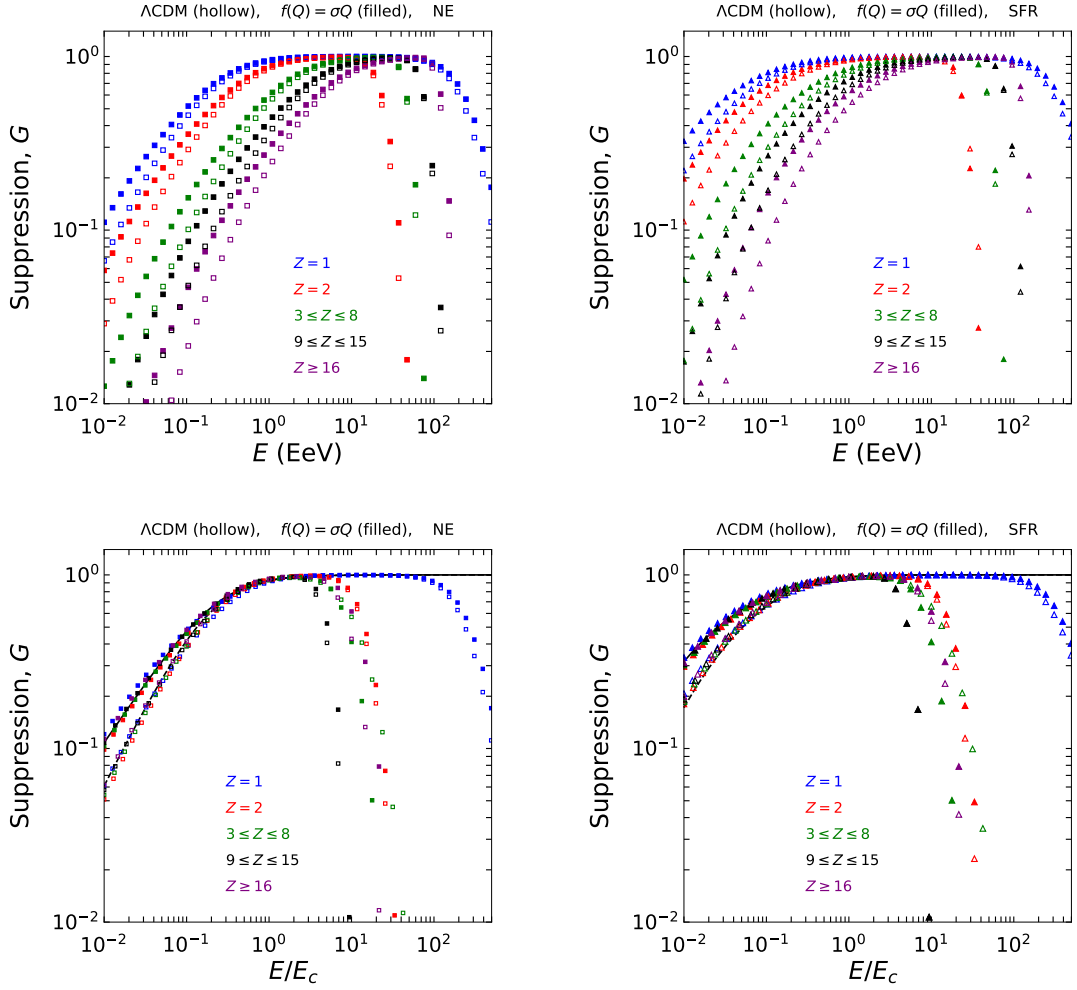


FIG. 9. Variations of suppression factor  $G$  with respect to the energy  $E$  (top panels) and  $E/E_c$  (bottom panels) for the different nuclei as predicted by the  $\Lambda$ CDM model and the  $f(Q)$  gravity model with NE and  $X_s = 1$ .

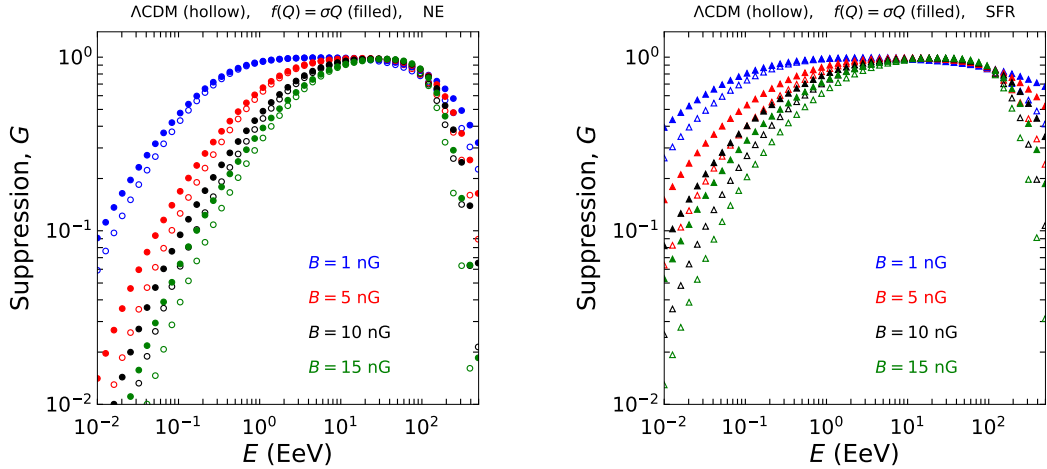


FIG. 10. Left: Variations of suppression factor with respect to the energy  $E$  for the different strengths of the magnetic field as predicted by the  $\Lambda$ CDM and the  $f(Q)$  gravity model with NE and  $X_s = 1$ . Right: Same as the left pane but for the SFR case.

field. For this analysis, we consider energy values ranging from  $E = 0.1$  EeV to  $E = 50$  EeV. The left and right panels of Fig. 11 depict the NE and SFR cases, respectively. The  $f(Q)$  gravity model predicts a higher degree of suppression compared to the

standard  $\Lambda$ CDM model. The influence of the cosmological model is apparent throughout the plot. However, as the TMF shifts to a higher strength, the model's effect becomes more. The CR flux suppression decreases quickly with increasing magnetic field strength for low-energy particles and it remains constant for substantially high-energy particles up to very high magnetic field strength as in the previous case.

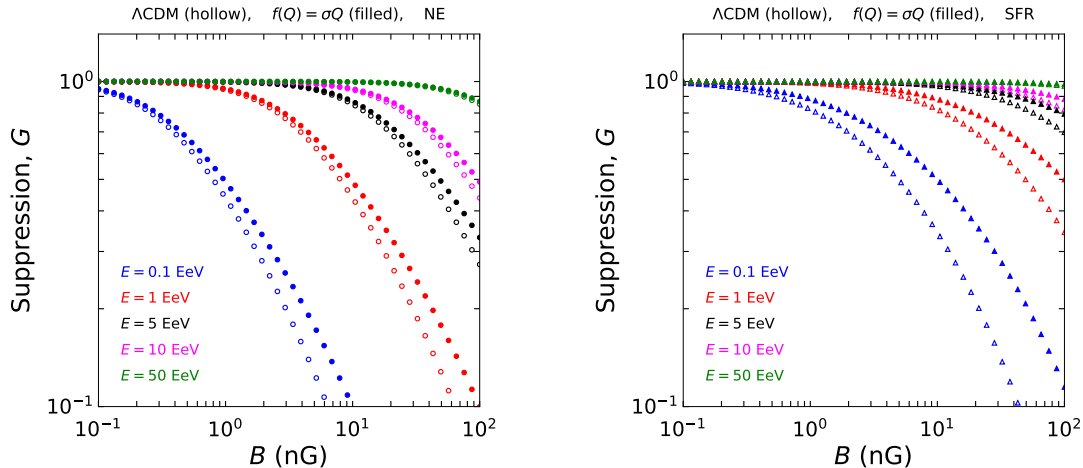


FIG. 11. Left: Variations of suppression factor with respect to the magnetic field for the different energy values as predicted by the  $\Lambda$ CDM and the  $f(Q)$  gravity model with NE and  $X_s = 1$ . Right: Same as the left pane but for the SFR case.

## VI. CONCLUSIONS

We study in detail the CR flux suppression in both low and high-energy regions through the magnetic horizon effect with the diffusion effect of CRs within the TMF. We consider a model for each of two MTGs for this analysis viz. the  $f(R)$  gravity and the  $f(Q)$  gravity. In the left panel of Fig. 1, we have shown the difference of the cosmological models through the Hubble parameter expression and in the right panel the cosmological time evolution with the redshift. We have calculated the magnetic suppression factor for all the cosmological models including the  $\Lambda$ CDM by considering the NE and SFR scenarios for different density sources  $X_s$  in Fig. 2 and 3. A scenario of the nuclei flux suppression as a function of both  $E$  and  $E/E_c$  is presented in detail in Fig. 4 and Fig. 5. We parameterize all these numerical results through an analytical factor  $P(E/E_c)$  given in Eq. (22). We consider the effect of the magnetic field in the suppression factor for all the cosmological models in Figs. 6 and 7. We discuss all of the above cases for the  $f(Q)$  gravity model in terms of Figs. 8 – 11 including NE and SFR scenarios. The effect of the cosmological model is better distinguished in the SFR case as compared to the case of NE.

In Fig. 12, we summarize the results of all three cosmological models for the study of the suppression factor in the case of NE (all panels) and  $X_s = 1$  (top right, bottom left and right panels). Since we have observed the same kind of patterns in SFR cases also, we have not included this scenario here. In the shaded regions, the upper boundary line denotes the results from the  $f(Q)$  gravity model (solid line), while the lower boundary line denotes the  $f(R)$  model (dash-dot line). The standard  $\Lambda$ CDM model (dotted line) lies between these two. From the top left panel, we can see that as the finite density of sources  $X_s$  increases, the cosmological model's effect in the high energy regime becomes narrower. In the top right panel, a scenario of the suppression factor is shown for the different primary particles as predicted by the considered cosmological models. From the bottom left panel, we can see that in between the magnetic field strength of 10 nG and 15 nG, all three cosmological models exhibit a similar kind of results in both low and high-energy regimes. Again from the bottom right panel, one can see that at the high energy regime, all considered cosmological models behave the same. Thus from this Fig. 12, we can conclude that the  $f(R)$  gravity power-law model exhibits low suppression results, the standard  $\Lambda$ CDM model exhibits a moderate suppression, and the  $f(Q)$  gravity model performs a higher suppression results in the UHECR flux.

The observations from the Pierre Auger Observatory indicate that as energy increases, heavier elements become more dominant in the CRs composition. To avoid the overlapping between different elements, strong suppression of heavy elements is necessary at lower energies. While elementary spectra with a very hard spectral index at the sources ( $\gamma < 1$ ) could explain this, it contradicts the expectations from second-order Fermi acceleration [45, 156]. An alternative explanation discussed in this present study involves a magnetic suppression effect, leading to a hardened spectrum for low rigidities. This effect could account for the observed composition and spectrum patterns with the spectral index at  $\gamma = 2$  [36, 157]. The MTGs play an effective role in explaining the behaviours of CR flux suppression in the Universe with accelerated expansion. The primary objective of this work is to investigate the potential impact of MTGs on the suppression of CR flux. The various predictions put

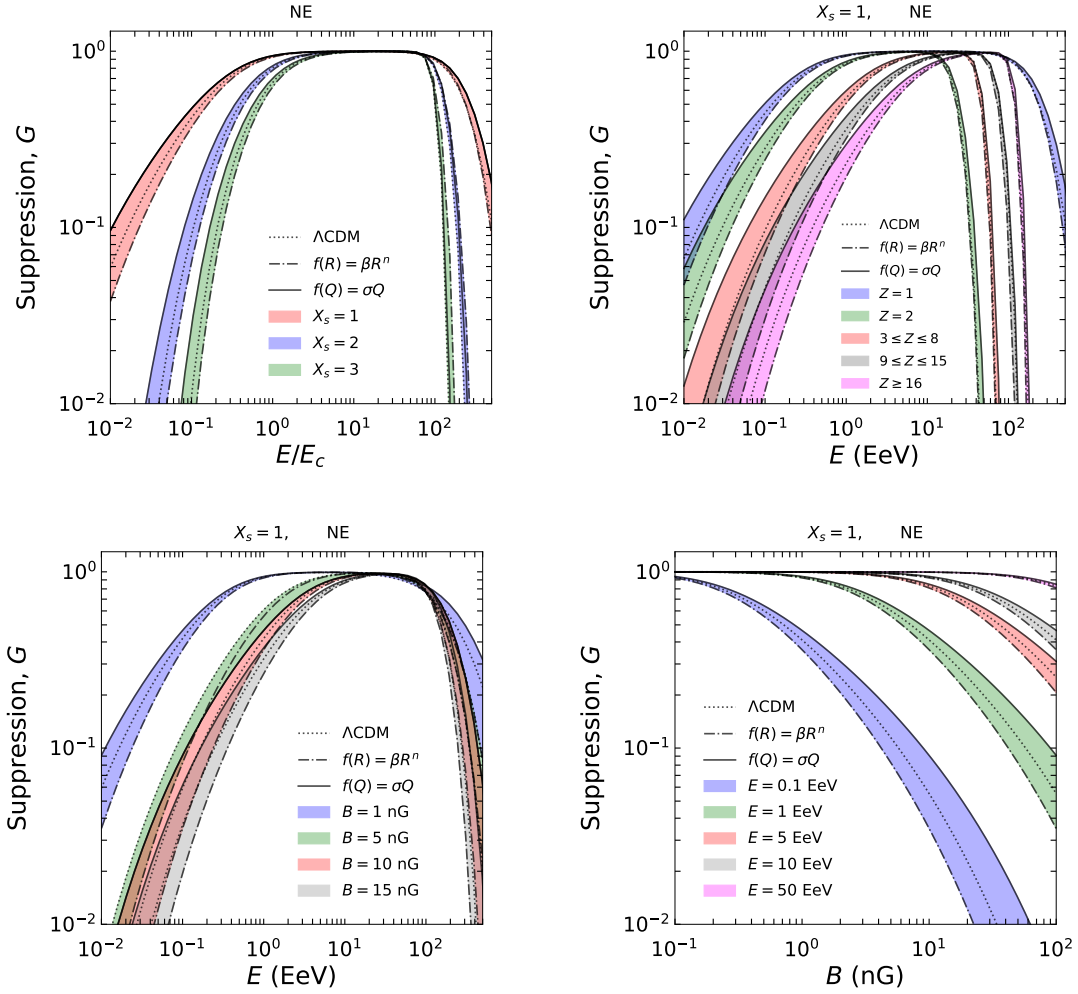


FIG. 12. Suppression factors for the different scenarios (see text) for the  $\Lambda$ CDM (dotted lines),  $f(R)$  gravity power-law (dash-dot lines), and  $f(Q)$  gravity model (solid lines) in NE case.

forth by these models highlight the need for further refinement in our comprehension of UHECR sources, their propagation, and the underlying principles of gravity. Moving forward, this study can be expanded by incorporating additional MTGs into both quantitative and more realistic analyses including secondary particles along with the primaries, aiming to gain deeper insights into the characteristics of CRs.

The extragalactic UHECRs that arrive from discrete sources differ from a continuous distribution across the space. At higher energies, the attenuation length of particles owing to interactions with the radiation backgrounds is comparable to the separation distance between the sources, resulting in a stronger suppression of flux. The background interactions can dramatically reduce the UHECR flux from nearby sources. This can have a significant impact on the CR flux recovery if the source spectrum extends beyond the attenuation limit [45]. Due to the magnetic horizon effect, the low energy flux gets suppressed from a discrete source distribution in the presence of a magnetic field. When particles like protons and nuclei come from space, they can be affected by the magnetic fields. If these particles have the same rigidity, which is related to their charge and energy, they will follow the same trajectory through these magnetic fields. Particles that keep their original masses experience more magnetic suppression when taken as a function of  $E/E_c$ , similar to what happens to protons [45]. Interestingly, even when particles lose some of their mass and charge during their journey as a result of photodisintegration, they mostly keep the same rigidity. This is because as their mass and charge decrease together, keeping their ratio the same. So, these secondary particles follow a trajectory through the magnetic field that is similar to that of the primary particles that exhibit without photodisintegration. We will study these secondary particles generated for different cosmological models in our next work.

## ACKNOWLEDGEMENTS

SPS is grateful to the authors of CRPropa and SimProp for making it available. UDG is thankful to the Inter-University Centre for Astronomy and Astrophysics (IUCAA), Pune, India for the Visiting Associateship of the institute.

- 
- [1] V. F. Hess, *Über Beobachtungen der durchdringenden Strahlung bei sieben Freiballonfahrten*, *Phys. Z.* **13**, 1084 (1912).
- [2] D. Harari, S. Mollerach, E. Roulet, *Anisotropies of ultrahigh energy cosmic rays diffusing from extragalactic sources*, *Phys. Rev. D* **89**, 123001 (2014) [arXiv:1312.1366].
- [3] S. Mollerach, E. Roulet, *Ultrahigh energy cosmic rays from a nearby extragalactic source in the diffusive regime*, *Phys. Rev. D* **99**, 103010 (2019) [arXiv:1903.05722].
- [4] V. Berezhinsky, A. Z. Gazizov, O. Kalashev, *Cascade photons as test of protons in UHECR*, *Astropart. Phys.*, **84**, 52 (2016) [arXiv:1606.09293].
- [5] V. Berezhinsky, A. Z. Gazizov, S. I. Grigorieva, *Signatures of AGN model for UHECR* [arXiv:astro-ph/0210095].
- [6] M. Nagano, A. A. Watson, *Observations and implications of the ultrahigh-energy cosmic rays*, *Rev. Mod. Phys.* **72**, 689 (2000).
- [7] P. Bhattacharjee, G. Sigl, *Origin and propagation of extremely high-energy cosmic rays*, *Phys. Rept.* **327** (2000) [arXiv:astro-ph/9811011].
- [8] A. V. Olinto, *Ultra High Energy Cosmic Rays: The theoretical challenge*, *Phys. Rept.* **333** (2000) [arXiv:astro-ph/0002006].
- [9] P. Blasi, *The Origin of Galactic Cosmic Rays*, *Astron. Astrophys. Rev.* **21**, 70 (2013), [arXiv:1311.7346].
- [10] E. G. Berezhko, H. Volk, *Spectrum of cosmic rays, produced in supernova remnants*, *Astrophys. J. Lett.* **661**, L175 (2007) [arXiv:0704.1715].
- [11] S. Mollerach, E. Roulet, *Anisotropies of ultrahigh-energy cosmic rays in a scenario with nearby sources*, *Phys. Rev. D* **105**, 063001 (2022) [arXiv:2111.00560].
- [12] P. Abreu et al. (Pierre Auger Collaboration), *Constraints on the origin of cosmic rays above  $10^{18}$  eV from large scale anisotropy searches in data of the Pierre Auger Observatory*, *Astrophys. J. Lett.* **762**, (2013) L13 [arXiv:1212.3083v1].
- [13] R. U. Abbasi (Telescope Array Collaboration), *Search for EeV Protons of Galactic Origin*, *Astropart. Phys.* **86**, 21 (2017) [arXiv:1608.06306v2].
- [14] M. G. Aartsen et al. (IceCube Collaboration), *Cosmic ray spectrum and composition from PeV to EeV using 3 years of data from IceTop and IceCube*, *Phys. Rev. D* **100**, 082002 (2019).
- [15] D. Ivanov et al. (Telescope Array Collaboration), *Energy Spectrum Measured by the Telescope Array Experiment*, *PoS ICRC* **298**, (2020).
- [16] P. Abreu et al. (Pierre Auger Collaboration), *The energy spectrum of cosmic rays beyond the turn-down around  $10^{17}$  eV as measured with the surface detector of the Pierre Auger Observatory*, *Eur. Phys. J. C* **81** (2021) 966 [arXiv:2109.13400v3].
- [17] V. Novotný, the Pierre Auger Collaboration, *Energy spectrum of cosmic rays measured using the Pierre Auger Observatory*, *PoS ICRC* **324** (2021).
- [18] K. Greisen, *End to the Cosmic-Ray Spectrum?*, *Phys. Rev. Lett.* **16**, 748 (1966).
- [19] G. T. Zatsepin, V. A. Kuzmin, *Upper Limit of the Spectrum of Cosmic Rays*, *JETP. Lett.* **4**, 78 (1966).
- [20] D. Harari, *Ultra-high energy cosmic rays*, *Phys. Dark Universe* **4**, 23 (2014).
- [21] J. Abraham et al. (The Pierre Auger Collaboration), *Observation of the Suppression of the Flux of Cosmic Rays above  $4 \times 10^{19}$  eV*, *Phys. Rev. Lett.* **101**, 061101 (2008) [arXiv:0806.4302v1].
- [22] R. U. Abbasi et al. (HiRes Collaboration), *First Observation of the Greisen-Zatsepin-Kuzmin Suppression*, *Phys. Rev. Lett.* **100** (2008) 101101 [arXiv:astro-ph/0703099v2].
- [23] T. Abu-Zayyad et al. (Telescope Array Collaboration), *The Cosmic-Ray Energy Spectrum Observed with the Surface Detector of the Telescope Array Experiment*, *Astrophys. J.* **768**, L1 (2013).
- [24] A. M. Hillas, *The energy spectrum of cosmic rays in an evolving universe*, *Phys. Lett. A*, **24**, 12 (1967).
- [25] K. Ptitsyna and S. Troitsky, *Lecture notes on high energy cosmic rays*, [arXiv:astro-ph/0808.0367].
- [26] M. Kachelriess, *Lecture notes on high energy cosmic rays*, [arXiv:astro-ph/0801.4376].
- [27] J. Abraham et al., (Pierre Auger Collaboration), *Upper limit on the cosmic-ray photon fraction at EeV energies from the Pierre Auger Observatory*, *Astropart. Phys.* **31**, 399 (2009) [arXiv:0903.1127v2].
- [28] T. Abu-Zayyad et al. (Telescope Array Collaboration), *Upper limit on the flux of photons with energies above  $10^{19}$  eV using the Telescope Array surface detector*, *Phys. Rev. D* **88**, 112005 (2013) [arXiv:1304.5614].
- [29] P. Abreu et al., (Pierre Auger Collaboration), *Search for Point-like Sources of Ultra-high Energy Neutrinos at the Pierre Auger Observatory and Improved Limit on the Diffuse Flux of Tau Neutrinos*, *Astrophys. J.* **755**, L4 (2012).
- [30] M. G. Aartsen et al., (IceCube Collaboration), *Search for a diffuse flux of astrophysical muon neutrinos with the IceCube 59-string configuration*, *Phys. Rev. D* **89**, 062007 (2014) [arXiv:1311.7048].
- [31] P. Abreu et al., (Pierre Auger Collaboration), *A Search for Point Sources of EeV Neutrons*, *Astrophys. J.* **760**, 148 (2012).
- [32] J. Abraham et al., (Pierre Auger Collaboration), *Measurement of the Depth of Maximum of Extensive Air Showers above  $10^{18}$  eV*, *Phys. Rev. Lett.* **104**, 091101 (2010) [arXiv:1002.0699v1].
- [33] Pierre Auger Collaboration, *Interpretation of the depths of maximum of extensive air showers measured by the Pierre Auger Observatory*, *JCAP* **02**, 026 (2013).

- [34] A. D. Supanitsky, *Cosmic ray propagation in the Universe in presence of a random magnetic field*, *JCAP* **04**, 046 (2021) [arXiv:2007.09063].
- [35] A. A. Halim et al., (Pierre Auger Collaboration), *Impact of the Magnetic Horizon on the Interpretation of the Pierre Auger Observatory Spectrum and Composition Data*, [arXiv:2404.03533].
- [36] S. Mollerach, E. Roulet, *Magnetic diffusion effects on the Ultra-High Energy Cosmic Ray spectrum and composition*, *JCAP* **10**, 013 (2013) [arXiv:1305.6519].
- [37] D. Wittkowski for The Pierre Auger Collaboration, *Reconstructed properties of the sources of UHECR and their dependence on the extragalactic magnetic field*, *PoS* **563** (ICRC2017).
- [38] M. Unger, G. R. Farrar, L. A. Anchordoqui, *Origin of the ankle in the ultra-high energy cosmic ray spectrum and of the extragalactic protons below it*, *Phys. Rev. D* **92**, 123001 (2015) [arXiv:1505.02153].
- [39] N. Globus, D. Allard, E. Parizot, *A complete model of the CR spectrum and composition across the Galactic to Extragalactic transition*, *Phys. Rev. D* **92**, 021302 (2015) [arXiv:1505.01377].
- [40] M. Lemoine, *Extra-galactic magnetic fields and the second knee in the cosmic-ray spectrum* *Phys. Rev. D* **71**, 083007 (2005) [arXiv:astro-ph/0411173].
- [41] V. Berezhinsky and A. Z. Gazizov, *Diffusion of Cosmic Rays in the Expanding Universe. II. Energy Spectra of Ultra-High Energy Cosmic Rays*, *Astrophys. J.* **669**, 684 (2007) [arXiv:astro-ph/0702102].
- [42] V. Berezhinsky, *Propagation and origin of ultra high-energy cosmic rays*, *Advances in Space Research* **41**, 2071 (2008).
- [43] N. Globus, D. Allard, E. Parizot, *Propagation of high-energy cosmic rays in extragalactic turbulent magnetic fields: resulting energy spectrum and composition*, *A & A.* **479**, 97 (2008) [arXiv:0709.1541].
- [44] R. Aloisio, V. Berezhinsky, *Diffusive Propagation of Ultra-High-Energy Cosmic Rays and the Propagation Theorem*, *Astrophys. J.* **612**, 900 (2004) [arXiv:astro-ph/0403095].
- [45] J. M. González, S. Mollerach, E. Roulet, *Magnetic diffusion and interaction effects on Ultrahigh Energy Cosmic Rays: protons and nuclei*, *Phys. Rev. D* **104**, 063005 (2021) [arXiv:2105.08138].
- [46] B. P. Abbott et al. (LIGO Scientific Collaboration and Virgo Collaboration), *Observation of Gravitational Waves from a Binary Black Hole Merger*, *Phys. Rev. Lett.* **116**, 061102 (2016) [arXiv:1602.03837].
- [47] The Event Horizon Telescope Collaboration et al., *First M87 Event Horizon Telescope Results. I. The Shadow of the Supermassive Black Hole*, *Astrophys. J. Lett.* **871**, L1 (2019).
- [48] The Event Horizon Telescope Collaboration et al., *First M87 Event Horizon Telescope Results. II. Array and Instrumentation*, *Astrophys. J. Lett.* **875**, L2 (2019).
- [49] The Event Horizon Telescope Collaboration et al., *First M87 Event Horizon Telescope Results. III. Data Processing and Calibration*, *Astrophys. J. Lett.* **875**, L3 (2019).
- [50] The Event Horizon Telescope Collaboration et al., *First M87 Event Horizon Telescope Results. IV. Imaging the Central Supermassive Black Hole*, *Astrophys. J. Lett.* **875**, L4 (2019).
- [51] The Event Horizon Telescope Collaboration et al., *First M87 Event Horizon Telescope Results. V. Physical Origin of the Asymmetric Ring*, *Astrophys. J. Lett.* **875**, L5 (2019).
- [52] The Event Horizon Telescope Collaboration et al., *First M87 Event Horizon Telescope Results. VI. The Shadow and Mass of the Central Black Hole*, *Astrophys. J. Lett.* **875**, L6 (2019).
- [53] A. G. Reiss et al., *Observational Evidence from Supernovae for an Accelerating Universe and a Cosmological Constant*, *Astron. J.* **116**, 1009 (1998) [arXiv:astro-ph/9805201].
- [54] S. Perlmutter et al., *Measurements of  $\Omega$  and  $\Lambda$  from 42 High-Redshift Supernovae*, *Astrophys. J.* **517**, 565 (1999) [arXiv:astro-ph/9812133].
- [55] D. N. Spergel et al., *Three-Year Wilkinson Microwave Anisotropy Probe ( WMAP ) Observations: Implications for Cosmology*, *Astrophys. J. Suppl. S* **170**, 377 (2007) [arXiv:astro-ph/0603449].
- [56] P. Astier et al., *The Supernova Legacy Survey: Measurement of  $\Omega_M$ ,  $\Omega_\Lambda$  and  $\omega$  from the First Year Data Set*, *A & A* **447**, 31 (2006) [arXiv:astro-ph/0510447].
- [57] G. Cognola et al., *A Class of viable modified  $f(R)$  gravities describing inflation and the onset of accelerated expansion*, *Phys. Rev. D* **77**, 046009 (2008) [arXiv:0712.4017].
- [58] E. J. Copeland, M. Sami, S. Tsujikawa, *Dynamics of dark energy*, *IJMP D* **15**, 1753-1936 (2006) [arXiv:hep-th/0603057].
- [59] U. D. Goswami, H. Nandan, M. Sami, *Formation of caustics in Dirac-Born-Infeld type scalar field systems*, *Phys. Rev. D* **82**, 103530 (2010).
- [60] S. D. Odintsov and V. K. Oikonomou, *Geometric Inflation and Dark Energy with Axion  $F(R)$  Gravity*, *Phys. Rev. D* **101**, 044009 (2020) [arXiv:2001.06830].
- [61] S. Nojiri, S. D. Odintsov and V. K. Oikonomou, *Unifying Inflation with Early and Late-time Dark Energy in  $F(R)$  Gravity*, *Phys. Dark Universe* **29**, 100602 (2020) [arXiv:1912.13128].
- [62] S. D. Odintsov and V. K. Oikonomou, *Unification of Inflation with Dark Energy in  $f(R)$  Gravity and Axion Dark Matter*, *Phys. Rev. D* **99**, 104070 (2019) [arXiv:1905.03496].
- [63] J. H. Oort, *The force exerted by the stellar system in the direction perpendicular to the galactic plane and some related problems*, *Bull. Astron. Inst. the Netherlands.* **6**, 249 (1932).
- [64] F. Zwicky, *Helv. Phys. Acta.* **6**, 110-127 (1933); F. Zwicky, *Republication of: The redshift of extragalactic nebulae*, *Gen. Relativ. Gravit.* **41**, 207224 (2009).
- [65] F. Zwicky, *On the Masses of Nebulae and of Clusters of Nebulae*, *Astrophys. J.* **86**, 217-246 (1937).
- [66] K. Garrett and G. Duda, *Dark Matter: A Primer*, *Adv. Astron.*, 968283 (2011) [arXiv:1006.2483].
- [67] N. Parbin, U. D. Goswami, *Galactic rotation dynamics in a new  $f(R)$  gravity model*, *Eur. Phys. J. C* **83**, 411 (2023) [arXiv:2208.06564].



- [68] S. Nojiri and S. D. Odintsov, *Unified cosmic history in modified gravity: from  $F(R)$  theory to Lorentz non-invariant models*, *Phys. Rept.* **505**, 59 (2011) [arXiv:1011.0544].
- [69] S. Nojiri, S. D. Odintsov and V. K. Oikonomou, *Modified Gravity Theories on a Nutshell: Inflation, Bounce and Late-time Evolution*, *Phys. Rept.* **692**, 1 (2017) [arXiv:1705.11098].
- [70] P. Sotiriou, V. Faraoni,  *$f(R)$  theories of gravity*, *Rev. Mod. Phys.* **82**, 451 (2010) [arXiv:0805.1726].
- [71] A. A. Starobinsky, *Disappearing cosmological constant in  $f(R)$  gravity*, *JETP. Lett.* **86**, 157 (2007) [arXiv:0706.2041].
- [72] A. A. Starobinsky, *A New Type of Isotropic Cosmological Models without Singularity*, *Phys. Lett. B* **91**, 99 (1980).
- [73] W. Hu and I. Sawicki, *Models of  $f(R)$  cosmic acceleration that evade solar system tests*, *Phys. Rev. D* **76**, 064004 (2007) [arXiv:0705.1158v1].
- [74] S. Tsujikawa, *Observational signatures of  $f(R)$  dark energy models that satisfy cosmological and local gravity constraints*, *Phys. Rev. D* **77**, 023507 (2008) [arXiv:0709.1391v2].
- [75] D. J. Gogoi, U. D. Goswami, *Gravitational Waves in  $f(R)$  Gravity Power Law Model*, *Indian J. Phys.* **96**, 637 (2022) [arXiv:1901.11277v3].
- [76] U. D. Goswami, K. Deka, *Cosmological Dynamics of  $f(R)$  Gravity Scalar Degree of Freedom in Einstein Frame*, *IJMP D* **22**, 13 (2013) 1350083 [arXiv:1303.5868].
- [77] J. B. Jiménez et al., *Coincident General Relativity*, *Phys. Rev. D* **98**, 044048 (2018) [arXiv:1710.03116].
- [78] T. Harko et al., *Coupling matter in modified  $Q$  gravity*, *Phys. Rev. D* **98**, 084043 (2018) [arXiv:1806.10437].
- [79] S. Mandal, P. K. Sahoo, J. R. L. Santos, *Energy conditions in  $f(Q)$  gravity*, *Phys. Rev. D* **102**, 024057 (2020) [arXiv:2008.01563].
- [80] S. Mandal, D. Wang, P. K. Sahoo, *Cosmography in  $f(Q)$  gravity*, *Phys. Rev. D* **102**, 124029 (2020) [arXiv:2011.00420].
- [81] N. Frusciante, *Signatures of  $f(Q)$  gravity in cosmology*, *Phys. Rev. D* **103**, 044021 (2021) [arXiv:2101.09242].
- [82] P. Sarmah, A. De, U. D. Goswami, *Anisotropic LRS-BI Universe with  $f(Q)$  gravity theory*, *Phys. Dark Universe* **40**, 101209 (2023) [arXiv:2303.05905].
- [83] D. J. Gogoi and U. D. Goswami, *A new  $f(R)$  Gravity Model and properties of Gravitational Waves in it*, *Eur. Phys. J. C* **80**, 1101 (2020) [arXiv:2006.04011].
- [84] J. Bora, D. J. Gogoi, U. D. Goswami, *Strange stars in  $f(R)$  gravity Palatini formalism and gravitational wave echoes from them*, *JCAP* **09**, 057 (2022) [arXiv:2204.05473v2].
- [85] N. Parbin et al., *Deflection angle, quasinormal modes and optical properties of a de Sitter black hole in  $f(T, B)$  gravity*, *Phys. Dark Universe* **42**, 101315 (2023) [arXiv:2211.02414].
- [86] B. Hazarika, P. Phukon, *Thermodynamic topology of black holes in  $f(R)$  gravity*, *Prog. Theor. Exp. Phys.* **2024**, 043E01 (2024), [arXiv:2401.16756v3].
- [87] N. Parbin, D. J. Gogoi, U. D. Goswami, *Weak gravitational lensing and shadow cast by rotating black holes in axionic Chern–Simons theory*, *Phys. Dark Universe* **41**, 101265 (2023) [arXiv:2305.09157].
- [88] R. Karmakar, D. J. Gogoi, U. D. Goswami, *Thermodynamics and shadows of GUP-corrected black holes with topological defects in Bumblebee gravity*, *Phys. Dark Universe* **41**, 101249 (2023) [arXiv:2303.00297].
- [89] R. Karmakar, U. D. Goswami, *Quasinormal modes, temperatures and greybody factors of black holes in a generalized Rastall gravity theory*, *Phys. Scr.* **99**, 055003 (2024) [arXiv:2310.18594].
- [90] M. Chakraborty et al., (Grapes-3 Collaboration), *Large-scale cosmic ray anisotropy measured by the GRAPES-3 experiment*, *PoS ICRC* **395** (2021).
- [91] N. Globus et al., *Cosmic ray anisotropy from large-scale structure and the effect of magnetic horizons*, *MNRAS* **484**, 4167 (2019).
- [92] H. Yoshiguchi et al., *Small-Scale Clustering in the Isotropic Arrival Distribution of Ultra-High-Energy Cosmic Rays and Implications for Their Source Candidates*, *Astrophys. J.* **586**, 1211 (2003).
- [93] S. Mollerach, E. Roulet, *Anisotropies of ultrahigh-energy cosmic rays in a scenario with nearby sources*, *Phys. Rev. D* **105**, 063001 (2022) [arXiv:2111.00560v2].
- [94] S. Mollerach, E. Roulet, O. Taborada, *Large-scale anisotropies of extragalactic cosmic rays below the ankle*, *JCAP* **12**, 021 (2022) [arXiv:2207.11540v2].
- [95] A. Aab et al. (Pierre Auger Collaboration), *Observation of a Large-scale Anisotropy in the Arrival Directions of Cosmic Rays above  $8 \times 10^{18}$  eV*, *Science* **357**, 1266 (2017) [arXiv:1709.07321v1].
- [96] A. U. Abeysekara et al., *All-sky Measurement of the Anisotropy of Cosmic Rays at 10 TeV and Mapping of the Local Interstellar Magnetic Field*, *Astrophys. J.* **871**, 96 (2019).
- [97] P. Mertsch, M. Ahlers, *Cosmic Ray Small-Scale Anisotropies in Quasi-Linear Theory*, *JCAP* **11**, 048 (2019) [arXiv:1909.09052v2].
- [98] M. Ahlers, P. Mertsch, *Origin of Small-Scale Anisotropies in Galactic Cosmic Rays*, *Prog. Part. Nucl. Phys.* **94**, 184 (2017) [arXiv:1612.01873v1].
- [99] D. Harari, S. Mollerach, E. Roulet, *Cosmic ray anisotropies from transient extragalactic sources*, *Phys. Rev. D* **103**, 023012 (2021) [arXiv:2010.10629v2].
- [100] P. Erdogdu et al., *The dipole anisotropy of the 2 Micron All-Sky Redshift Survey*, *MNRAS* **368**, 1515 (2006).
- [101] A. Y. Prosekin, S. R. Kelner, F. A. Aharonian, *Transition of propagation of relativistic particles from the ballistic to the diffusion regime*, *Phys. Rev. D* **92**, 083003 (2015) [arXiv:1506.06594].
- [102] S. Mollerach, E. Roulet, *Ultrahigh energy cosmic rays from a nearby extragalactic source in the diffusive regime*, *Phys. Rev. D* **99**, 103010 (2019) [arXiv:1903.05722v2].
- [103] G. Sigl, M. Lemoine, and P. Biermann, *Ultra-high energy cosmic ray propagation in the local supercluster*, *Astropart. Phys.* **10**, 141 (1999).
- [104] V. Berezhinsky, A. Z. Gazizov, *Diffusion of Cosmic Rays in the Expanding Universe. I.*, *Astrophys. J.* **643**, 8 (2006) [arXiv:astro-ph/0512090].

- [105] D. J. Bird et al., *Detection of a Cosmic Ray with Measured Energy Well beyond the Expected Spectral Cutoff due to Cosmic Microwave Radiation*, *Astrophys. J.* **441** (1995) [arXiv:astro-ph/9410067].
- [106] V. Berezhinsky, A. Z. Gazizov, S. I. Grigorieva, *Dip in UHECR spectrum as signature of proton interaction with CMB*, *Phys. Lett. B* **612**, 147 (2005) [arXiv:astro-ph/0502550].
- [107] V. Berezhinsky, A. Z. Gazizov, S. I. Grigorieva, *On astrophysical solution to ultrahigh energy cosmic rays*, *Phys. Rev. D* **74**, 043005 (2006) [arXiv:hep-ph/0204357].
- [108] V. A. Semenov, A. V. Kravtsov, D. Caprioli *Cosmic-Ray Diffusion Suppression in Star-forming Regions Inhibits Clump Formation in Gas-rich Galaxies*, *Astrophys. J.* **910**, 126 (2021).
- [109] A. L. Mesquita, D. Rodgers-Lee, A. A. Vidotto, R. D. Kavanagh, *The strong suppression of galactic cosmic rays reaching AU Mic b, c, and Prox Cen b*, *MNRAS* **515**, 1218 (2022).
- [110] The High Resolution Fly's Eye Collaboration, *Monocular Measurement of the Spectrum of UHE Cosmic Rays by the FADC Detector of the HiRes Experiment*, *Astropart. Phys.* **23**, 157 (2005) [arXiv:astro-ph/0208301].
- [111] M. Takeda et al., *Energy determination in the Akeno Giant Air Shower Array experiment*, *Astropart. Phys.* **19**, 447 (2003) [arXiv:astro-ph/0209422].
- [112] A. Aab et al. (Pierre Auger Collaboration), *Inferences on mass composition and tests of hadronic interactions from 0.3 to 100 EeV using the water-Cherenkov detectors of the Pierre Auger Observatory*, *Phys. Rev. D* **96**, 122003 (2017).
- [113] A. Aab et al. (Pierre Auger Collaboration), *Large-scale Cosmic-Ray Anisotropies above 4 EeV Measured by the Pierre Auger Observatory*, *Astrophys. J.* **868**, 4 (2018).
- [114] D. Ivanov (Telescope Array Collaboration), *Energy Spectrum Measured by the Telescope Array Experiment*, *Proc. Sci. ICRC 2019*, **298** (2019).
- [115] A. Aab et al. (Pierre Auger Collaboration) *Measurement of the cosmic-ray energy spectrum above  $2.5 \times 10^{18}$  eV using the Pierre Auger observatory*, *Phys. Rev. D* **102**, 062005 (2020) [arXiv:2008.06486].
- [116] M. Honda et al. (Akeno Collaboration), *Inelastic cross section for p-air collisions from air shower experiments and total cross section for p-p collisions up to  $\sqrt{s} = 24$  TeV*, *Phys. Rev. Lett.* **70**, 525 (1993).
- [117] R. U. Abbasi et al. (HiRes Collaboration), *A Study of the Composition of Ultra-High-Energy Cosmic Rays Using the High-Resolution Fly's Eye*, *Astrophys. J.* **622**, 910 (2005).
- [118] The Pierre Auger Collaboration, *First Estimate of the Primary Cosmic Ray Energy Spectrum above 3 EeV from the Pierre Auger Observatory*, *Proc. 29th ICRC, August 3-10, 2005, Pune, India* [astro-ph/0507150].
- [119] The Pierre Auger Collaboration et al., *Testing effects of Lorentz invariance violation in the propagation of astroparticles with the Pierre Auger Observatory*, *JCAP* **01**, 023 (2022) [arXiv:2112.06773].
- [120] D. R. Bergman et al., (Pierre Auger and Telescope Array Collaborations), *The energy spectrum of ultra-high energy cosmic rays measured at the Pierre Auger Observatory and the Telescope Array*, *Eur. Phys. J Web Conf.* **283**, 02003 (2023).
- [121] P. L. Biermann, V. Souza, *Centaurus A: The Extragalactic Source of Cosmic Rays with Energies above the Knee*, *Astrophys. J.* **746**, 72 (2012).
- [122] S. P. Sarmah, U. D. Goswami, *Propagation and Fluxes of Ultra High Energy Cosmic Rays in  $f(R)$  Gravity Theory*, *Eur. Phys. J. C* **84**, 419 (2024) [arXiv:2303.16678].
- [123] S. P. Sarmah, U. D. Goswami, *Anisotropies of Diffusive Ultra-high Energy Cosmic Rays in  $f(R)$  Gravity Theory*, *Astroparticle Physics* **163** (2024) 103005 [arXiv:2309.14361].
- [124] J. L. Han, *Observing Interstellar and Intergalactic Magnetic Fields*, *Annu. Rev. Astron* **255**, 111 (2017).
- [125] Y. Hu et al., *Turbulent Magnetic Field Amplification by the Interaction of a Shock Wave and Inhomogeneous Medium*, *Astrophys. J.* **941**, 133 (2022).
- [126] U. Chadayammuri, *Turbulent magnetic fields in merging clusters: a case study of Abell 2146*, *MNRAS* **512**, 2 (2022).
- [127] L. Feretti et al., *Clusters of galaxies: observational properties of the diffuse radio emission*, *Astron. Astrophys. Rev.* **20**, 54 (2012).
- [128] J. P. Vallée, *A Synthesis of Fundamental Parameters of Spiral Arms, Based on Recent Observations in the Milky Way*, *New Astro. Rev.* **55**, 91 (2011).
- [129] F. Vazza et al., *Simulations of extragalactic magnetic fields and of their observables*, *Class. Quantum Grav.* **34**, 234001 (2017).
- [130] G. Sigl, F. Miniati and T. A. Ensslin, *Ultrahigh energy cosmic ray probes of large scale structure and magnetic fields*, *Phys. Rev. D* **70**, 043007 (2004) [arXiv:astro-ph/0401084].
- [131] D. Allard, *Extragalactic propagation of ultrahigh energy cosmic-rays*, *Astropart. Phys.* **39-40**, 33 (2012) [arXiv:1111.3290].
- [132] D. J. Gogoi and U. D. Goswami, *Cosmology with a new  $f(R)$  gravity model in Palatini formalism*, *IJMP D* **31**, 2250048 (2022) [arXiv:2108.01409].
- [133] B. Santos, M. Campista, J. Santos, J. S. Alcaniz, *Cosmology with Hu-Sawicki gravity in the Palatini formalism*, *A & A* **548**, A31 (2012) [arXiv:1207.2478].
- [134] N. Aghanim et al., *Planck 2018 results* (Planck Collaboration), *A & A* **641**, A6 (2020) [arXiv:1807.06209].
- [135] K. Nakamura and Particle Data Group, *Review of Particle Physics*, *J. Phys. G: Nucl. Part. Phys.* **37**, 075021(2010).
- [136] R. Solanki et al., *Cosmic acceleration with bulk viscosity in modified  $f(Q)$  gravity*, *Phys. Dark Universe*, **32**, 100820 (2021), [arXiv:2105.00876].
- [137] K. Kotera and M. Lemoine, *Optical depth of the Universe to ultrahigh energy cosmic ray scattering in the magnetized large scale structure*, *Phys. Rev. D* **77**, 023005 (2008) [arXiv:0801.1450].
- [138] H. Yoshiguchi et al., *Small-Scale Clustering in the Isotropic Arrival Distribution of Ultra-High-Energy Cosmic Rays and Implications for Their Source Candidates*, *Astrophys. J.* **586**, 1211 (2003).
- [139] M. Lemoine, *Extra-galactic magnetic fields and the second knee in the cosmic-ray spectrum*, *Phys. Rev. D* **71**, 083007 (2005) [arXiv:astro-ph/0411173].

- [140] D. Hooper, S. Sarkar, A. M. Taylor, *The intergalactic propagation of ultra-high energy cosmic ray nuclei*, *Astropart. Phys.* **27**, 199 (2007).
- [141] *The Intergalactic Propagation of Ultra-High Energy Cosmic Ray Nuclei: An Analytic Approach*, *Phys. Rev. D* **77**, 103007 (2008) [arXiv:0802.1538].
- [142] P. Blasi and A. V. Olinto, *Magnetized local supercluster and the origin of the highest energy cosmic rays*, *Phys. Rev. D* **59**, 023001 (1999).
- [143] T. Stanev et al., *Propagation of ultrahigh energy protons in the nearby universe*, *Phys. Rev. D* **62**, 093005 (2000) .
- [144] G. Sigl, *Nonuniversal spectra of ultrahigh energy cosmic ray primaries and secondaries in a structured universe*, *Phys. Rev. D* **75**, 103001 (2007) [arXiv:astro-ph/0703403].
- [145] R. Aloisio *Acceleration and propagation of ultra high energy cosmic rays*, *Prog. Theor. Exp. Phys.* **2017**, 12A102 (2017) [arXiv:1707.08471]
- [146] S. I. Syrovatskii, *The Distribution of Relativistic Electrons in the Galaxy and the Spectrum of Synchrotron Radio Emission*, *Soviet Astro.* **3**, 22 (1959).
- [147] R. A. Batista, G. Sigl, *Diffusion of cosmic rays at EeV energies in inhomogeneous extragalactic magnetic fields*, *JCAP* **11**, 031 (2014) [arXiv:1407.6150].
- [148] P. Virtanen et al., *SciPy 1.0: fundamental algorithms for scientific computing in Python*, *Nature Methods* **17**, 261 (2020).
- [149] R. A. Batista et al., *CRPropa 3.2 – an advanced framework for high-energy particle propagation in extragalactic and galactic spaces*, *JCAP* **09**, 035 (2022) [arXiv:2208.00107].
- [150] R. Aloisio et al., *SimProp v2r4: Monte Carlo simulation code for UHECR propagation*, *JCAP* **11**, 009 (2017) [arXiv:1705.03729].
- [151] A. M. Hopkins, J. F. Beacom, *On the Normalization of the Cosmic Star Formation History*, *Astrophys. J.* **651**, 142 (2006) [arXiv:astro-ph/0601463].
- [152] A. M. Taylor, M. Ahlers and F. A. Aharonian, *Need for a local source of ultrahigh-energy cosmic-ray nuclei*, *Phys. Rev. D* **84**, 105007 (2011).
- [153] J. H. Matthews, A.R. Bell, K.M. Blundell and A.T. Araudo, *Fornax A, Centaurus A, and other radio galaxies as sources of ultrahigh energy cosmic rays*, *MNRAS Lett.* **479**, L76 (2018).
- [154] R. Guedes Lang, A. M. Taylor, M. Ahlers and V. de Souza, *Revisiting the distance to the nearest ultrahigh energy cosmic ray source: Effects of extragalactic magnetic fields*, *Phys. Rev. D* **102** 063012 (2020).
- [155] M. Kachelriess, P. Serpico, *The Compton–Getting effect on ultra-high energy cosmic rays of cosmological origin*, *Phys. Lett. B* **640**, 225 (2006)
- [156] A. Aab et al. (Pierre Auger Collaboration), *Combined fit of spectrum and composition data as measured by the Pierre Auger Observatory*, *JCAP* **04**, 038 (2017) [arXiv:1612.07155].
- [157] S. Mollerach, E. Roulet, *Extragalactic cosmic rays diffusing from two populations of sources*, *Phys. Rev. D* **101**, 103024 (2020) [arXiv:2004.04253].